Danish Meteorological Institute
Ministry of Transport

Scientific Report 04-06

CONTRAILS AND THEIR IMPACT ON CLIMATE

Annette Guldberg and Johannes K. Nielsen

Colophone

Serial title:
Scientific Report 04-06

Title:
CONTRAILS AND THEIR IMPACT ON CLIMATE

Subtitle:

Authors:
Annette Guldberg and Johannes K. Nielsen

Other Contributers:

Responsible Institution:
Danish Meteorological Institute

Language:
English

Keywords:
IFSHAM, contrail parameterization, MPC model, microphysics

Url:
www.dmi.dk/dmi/sr04-06

ISSN:
139-1949

ISBN:
87-7478-507-9

Version:

Website:
www.dmi.dk

Contents

Dansk resume

Dette er den afsluttende rapport for projektet “Civil flytrafiks indflydelse på atmosfæren” påbegyndt på DMI i 2001. Rapporten redegør for nogle af de resultater, som er opnået på DMI under dette projekt. [1]

Den helt store usikkerhed på estimater af flytrafikkens indvirkning på klimaet findes i påvirkningen gennem partikler produceret af flyvemaskiner [Sausen et al., 2004]. Partikeludsendelsen muliggør dannelsen af kondensstriber, der kan udvikle sig til egentlige cirrusskyer, og der er meget stor usikkerhed på bestemmelsen af disse skyformers klimapåvirkning. En metode til bestemmelse af kondensstribers klimapåvirkning er simuleringer med globale klimamodeller, der indeholder en beskrivelse (parameterisering) af kondensstriber. Hidtil har der kun eksisteret en enkelt model med en sådan parameterisering, [Ponater et al., 2002, Marquart and Mayer, 2002], nemlig ECHAM4. Parameteriseringen fra ECHAM4 er i dette projekt blevet implementeret i IFSHAM-modellen, hvilket muliggør en analyse af, hvordan beskrivelsen af kondensstriberne og deres egenskaber afhænger af den anvendte model. En væsentlig forskel mellem de to modeller er, at den globale netto strålingspåvirkning fra kondensstriber er næsten en størrelsesorden mindre i IFSHAM, men ikke mindst at netto strålingspåvirkningen er positiv overalt på kloden i ECHAM4, mens der er store områder over Europa og USA, hvor netto påvirkningen er negativ i IFSHAM. Partiklernes effektive radius beskrives ikke ens i de to modeller. Ændres beskrivelsen i IFSHAM, således at den bliver identisk med beskrivelsen i ECHAM4, fører det til en øgning af netto strålingspåvirkningen med en faktor 2, men den er stadig væsentlig mindre end i ECHAM4 modellen, og det geografiske mønster ændres ikke - der er stadig områder over USA og Europa med negativ strålingspåvirkning. Følsomheden overfor den optiske dybde har været undersøgt ved at vælge konstante værdier for den optiske dybde. Dette har stor betydning for strålingspåvirkningen og fører til resultater, der er i bedre overensstemmelse med resultaterne fra ECHAM4, men det er et spørgsmål hvor realistisk de konstante optiske dybder er.

Udover en sammenligning af de to modellers resultater, har betydningen af modellens (IFSHAM) systematiske fejl for kondensstribernes egenskaber været analyseret ved hjælp af den såkaldte nudging-teknik. En vis øgning i strålingspåvirkningen ses, når modellens systematiske fejl minimeres.

For at belyse problemet med de to globale modellers bud på partiklernes effektive radius er der blevet udført simuleringer af kondensstriber med DMI’s mikrofysiske cirrus model, (MPC-modellen) [Nielsen, 2004] på enkelte lokaliteter, med henblik på at sammenligne IFSHAM simuleringerne med en mere detaljeret mikrofysisk cirrus beskrivelse. Også størrelsen af den optiske dybde er blevet undersøgt. MPC simuleringerne er udført ved forskellige atmosfæriske betingelser, og simuleringerne viser at skyfysikken er meget følsom over for initial vanddamp og temperatur variationer. Men selv om denne følsomhed tages i betragtning, peger MPC-simuleringerne på, at der er større variabilitet i partikelstørrelsen end ECHAM4 parameteriseringen implicerer, altså at IFSHAM parameteriseringen er mest realistisk. MPC-modellen bekræfter også, at den effektive radius i flykondensstriber er størst i troperne, og aftager mod polerne.

[1] En mere detaljeret (dansksproget) redegørelse omhandlende den internationale status af forskningsområdet som sådan år 2004, findes i Klima Center rapport 04-04 “Flytrafiks indflydelse på atmosfæren”, DMI 2004.

Abstract

The airplane contrail parameterization scheme of [Ponater et al., 2002], used in the global climate model ECHAM4, is implemented in the IFSHAM model. Results from simulations with the two models are compared with respect to radiative forcing of contrails and contrail optical properties. The main difference between the two models is that the global mean of the net radiative forcing is almost a factor of ten less in the IFSHAM model and that there are large areas over Europe and USA, where the net radiative forcing is negative. In ECHAM4 the net forcing is positive everywhere. Concerning optical properties the size and the geographical pattern of the particle effective radius is rather different in the two models and the magnitude of the optical depth has a large impact on the contrail radiative forcing. Besides comparing the results of the two models also the impact of model systematic errors has been studied using the socalled nudging technique. The problem of the model differences in determining the particle effective radius as well as the magnitude of the optical depth is further investigated with the cloud resolving microphysical cirrus model (MPC-model) of DMI. The MPC model simulations confirm the IFSHAM parameterization in the sense that the variability of effective radius indeed is rather large (5-45 μ m), and that effective radius is much larger in tropical contrails than in midlatitude and arctic contrails.

Introduction

Line-shaped contrails and cirrus developed from line-shaped contrails have an impact on the radiation balance of the Earth and therefore on the Earth's climate system. In 1999 the International Panel of Climate Change (IPCC) released the special report "Aviation and the global atmosphere", [IPCC, 1999]. In this report the best estimate of the radiative forcing of line-shaped contrails in 1992 is 0.02 W/m^2, with an uncertainty factor of 3 to 4. The estimate was based on radiative transfer calculations using a global contrail cover obtained from model calculations, but scaled to observed contrail cover in the Atlantic/European area, and using a constant value for the optical depth of contrails, [Minnis et al., 1999]. In 1999 there had been no attempt to include a description of contrails in global climate models. The first parameterization of contrails was developed by [Ponater et al., 2002] and implemented in the ECHAM4 general circulation model (GCM), [Roeckner et al., 1996]. Using the ECHAM4 model extended with the contrail parameterization the global radiative forcing of contrails in 1992 is estimated to 0.0035 W/m^2, [Marquart et al., 2003]; more than 5 times less than the estimate in the IPCC report from 1999. The advantage of using a general circulation model including a contrail parameterization is that contrail coverage and the optical properties of contrails are determined by the instantaneous atmospheric state. When using e.g. a radiative transfer model for obtaining global radiative forcing, specifications of typical mean atmospheric conditions and typical mean contrail properties are needed as input, and it is therefore not possible to account for the many different parameter combinations that can occur in different areas and different seasons [Ponater et al., 2002]. On the other hand general circulation models do have systematic errors, their resolution is crude and it is well known that the parameterizations of clouds need improvements.

The [Ponater et al., 2002] contrail parameterization has at DMI been implemented in the IFSHAM model with the purpose of studying the behaviour of contrails in a different model environment. The contrail behaviour has been analysed with respect to the optical properties of the contrails and to radiation parameterizations. Using the socalled nudging technique the impact of the systematic errors of the model on contrail properties has been investigated.

The radiative impact of contrails depends strongly on the optical properties of the contrails and the present knowledge of these properties is not sufficient. Both estimates obtained by observations and modelled estimates have huge uncertainties. An important tool for determining contrail optical properties is microphysical modelling of contrail development. In the second part of this report we present a microphysical cirrus model, the MPC model of DMI, and employ it on specific contrail events in order to evaluate the cloud parameterizations.

Climate modelling of contrails

Introduction

The climate impact of contrails can be studied using global climate models extended with a description of contrails as a tool. So far only one parameterization of contrails has been developed, namely the parameterization of [Ponater et al., 2002] for the ECHAM4 model. The behaviour of the contrail scheme may depend on the actual climate model used. For example the radiation scheme of the model may be important, as well as the parameterizations used for cloud optical properties. In the study described here the [Ponater et al., 2002] contrail parameterization has been implemented in the IFSHAM general circulation model. The IFSHAM model is developed at DMI by Shuting Yang, [Yang, 2004], as a combination of the dynamical core from the ARPEGE/IFS model, [Déqué et al., 1994], and the physical parameterization package from the ECHAM5 model, [Roeckner et al., 2003]. The purpose of implementing the contrail parameterization in a model different from the one used in [Ponater et al., 2002] is to study the model dependency of the contrail scheme. The two models have different dynamical cores, many of the physical parameterization schemes are changed from ECHAM4 to ECHAM5, and furthermore the two models are run in different resolution.

Global climate models are not perfect models, but suffer from long term systematic errors. These systematic errors may impact the properties of the contrails and thereby the contrail impact on the radiation balance. In order to study this a technique called 'nudging' has been applied. Using the nudging technique the model is forced to follow observed data closely, thereby minimizing the systematic errors of the model. Comparing experiments with the model in nudged mode and the free model, the importance of the systematic errors of the model for contrail behavior is investigated.

The next two sections of this chapter contain a description of the contrail parameterization and the model used - the IFSHAM model - followed by results from experiments with the IFSHAM model compared to the results of [Ponater et al., 2002]. Then two sections are describing the nudging technique and results of experiments with the model in nudged mode compared to results from free model runs. Conclusions are drawn and outlook for future developments are listed in the last section of this chapter.

Parameterizing contrails

Contrails can form in the atmosphere when the ambient air is sufficiently cold and humid. For contrails to form and persist temperatures below approximately -39 °C and supersaturation with respect to ice are required [Minnis et al., 2004]. If the air is supersaturated with respect to water, contrails can form, but unless the ambient air is supersaturated with respect to ice, they will disappear shortly after. Due to the required atmospheric conditions for contrail formation, contrails typically occur at altitudes between 8 and 12 km.

The basic thermodynamic theory for determining the conditions for contrail formation was developed by Schmidt and Appleman, [Schmidt, 1941] and [Appleman, 1953]. According to the thermodynamic theory threshold values for temperature, T_{contr}, and relative humidity (with respect to water), $r_{contr}(T)$ are determined. The meaning of these threshold values is, that contrails cannot form if the temperature is larger than T_{contr} and if the humidity (for a given temperature) is less than $r_{contr}(T)$. The [Ponater et al., 2002] contrail parameterization is based on the following approximation for T_{contr} (unit °C)

$$T_{contr} = -46.46 + 9.43ln(G - 0.053) + 0.72[ln(G - 0.053)]^2 \quad (3.1)$$

where G has the unit Pa/K and is defined as

$$G = (EI_{H_2O} c_p p)/[\epsilon Q(1 - \eta)] \quad (3.2)$$

EI_{H_2O} is the emission index of water, c_p the specific heat at constant pressure, p is pressure, ϵ the ratio of the molecular masses of water and air, Q the specific combustion heat and η the propulsion efficiency of the jet engine. The relative humidity threshold is given by

$$r_{contr}(T) = [G(T - T_{contr}) + e^L_{sat}(T_{contr})]/e^L_{sat}(T) \quad (3.3)$$

where e^L_{sat} is the saturation pressure of water vapor with respect to the liquid phase. For more information on this approximation of the threshold values see [Schumann, 1996] and [Schumann, 2000].

A parameterization of contrails has to be linked to the cloud parameterization of the GCM into which it is implemented. The [Ponater et al., 2002] contrail parameterization was implemented in the ECHAM4 model, where the cloud scheme is based on the parameterization developed by Sundqvist, [Sundqvist, 1978] and [Sundqvist et al., 1989]. The prognostic variables in the ECHAM4 cloud parameterization are water vapour mixing ratio and cloud water mixing ratio. A fractional cloud cover, b, is calculated according to

$$b = 1 - \sqrt{1 - \frac{r - r_{crit}}{r_{sat} - r_{crit}}} \quad (3.4)$$

if $r \geq r_{crit}$. If $r < r_{crit}$ b is set to 0. At altitudes where contrails form, clouds consist of ice particles, so at these altitudes r is the relative humidity with respect to ice and r_{sat} the relative saturation humidity with respect to ice. r_{crit} is an altitude dependent threshold value for cloud formation.

b is calculated for each grid box of the model and the water vapour is divided in two parts, one for the cloud covered part of the grid box, where saturation is assumed, and one for the cloud free part. In situations where supersaturation arises, the water vapour in excess is converted into cloud water. Cloud water is evaporated if the air is no longer saturated in the cloud covered part of a grid box.

The basic idea in the [Ponater et al., 2002] contrail parameterization is to define a threshold value for contrail formation, r^*_{crit}, as

$$r^*_{crit} = r_{crit} r_{contr} \quad (3.5)$$

Contrails can form for lower values of the relative humidity than normal cirrus clouds consistent with r^*_{crit} being less than r_{crit}. Using r^*_{crit} in equation 3.4 the total cover of high clouds, both contrails and natutal cirrus clouds, are determined as

$$b_{total} = 1 - \sqrt{1 - \frac{r - r^*_{crit}}{r_{sat} - r^*_{crit}}} \quad (3.6)$$

if $r \geq r^*_{crit}$. If $r < r^*_{crit}$ b_{total} is set to 0. The contrail cover can then be estimated as

$$b^{pot}_{contr} = b_{total} - b \quad (3.7)$$

It should be emphasized that the contrail cover determined in this way is the potential contrail cover. In order to obtain the actual contrail cover the potential contrail cover has to be weighted by the air traffic density. The actual contrail cover is determined by

$$b_{contr} = \gamma F b^{pot}_{contr} \quad (3.8)$$

F is the local amount of aircraft fuel consumption and γ is a tuning parameter for adjusting the calculated contrail cover to the observed contrail cover. Persistent contrails are considered in this parameterization by requiring that supersaturation with respect to ice is occuring in the contrail covered part of a grid box. If the humidity is less than the saturation value in the contrail covered part of a grid box the contrail ice water will evaporate within a model time step and the contrail coverage is set to 0. Optical properties of the contrails are determined using the same parameterizations as used for natural cirrus clouds.

The [Ponater et al., 2002] contrail parameterization is a diagnostic determination of contrails and their properties. There is no feedback of the contrails to the modelled climate. For a more detailed description of the contrail parameterization and its implementation in the ECHAM4 model, see [Ponater et al., 2002].

The general circulation model used

The [Ponater et al., 2002] contrail parameterization has at DMI been implemented in the IFSHAM general circulation model. The IFSHAM model is a combination of the dynamical core from the ARPEGE/IFS [Déqué et al., 1994], version 3, model and the physical parameterization package from the ECHAM5 model [Roeckner et al., 2003], and has been developed at DMI, [Yang, 2004]. The model is a spectral primitive equation model and the equations are solved using the transform method [Eliasen et al., 1970], semi-Lagrangian advection and a two-level semi-implicit time stepping scheme. The ECHAM4 model used by [Ponater et al., 2002] is also a spectral primitive equation model, but here Eulerian advection and a three-level time stepping scheme is applied.

The physical parameterization package of the ECHAM5 model and therefore also of the IFSHAM model contains the possibility for choosing between two cloud schemes: a prognostic, statistical scheme by [Tompkins, 2002] and a scheme based on the [Sundqvist, 1978] ideas. Because the [Ponater et al., 2002] contrail parameterization as mentioned above is linked to the Sundqvist cloud scheme, the Sundqvist scheme has to be chosen when extending the IFSHAM model with the contrail parameterization. Although the basic principles of the cloud scheme are the same in the ECHAM4 model version used by [Ponater et al., 2002] and the ECHAM5 model some changes have been made in the ECHAM5 version. For a detailed description of these modifications, see [Lohmann and Roeckner, 1996]. The main difference between the ECHAM5 and the ECHAM4 version is that in the ECHAM5 version cloud water and cloud ice are treated as two seperate prognostic variables. In ECHAM4 there is only one prognostic variable for cloud water and cloud ice together, and cloud water and ice are then seperated diagnostically based on temperature. Semi-Lagrangian advection is used in the IFSHAM model, and as semi-Lagrangian advection schemes are not mass conserving, mass loss is a problem when advecting positive definite quantities like cloud water and ice. Therefore the advection of cloud water and ice has been turned off in the experiments described here.

A very important difference between the physics of the ECHAM4 and the IFSHAM models in relation to contrail properties is the radiation schemes used in the two models. The ECHAM4 model is using the scheme by [Fouquart and Bonnel, 1980] for the short wave spectrum and the scheme by [Morcrette, 1991] for the long wave spectrum. The IFSHAM model is also using the [Fouquart and Bonnel, 1980] scheme for the short wave spectrum but extended from two to four spectral intervals. For the long wave spectrum the Rapid Radiative Transfer Model (RRTM) by [Mlawer et al., 1997] is used in the IFSHAM model.

The ECHAM4 model as used in [Ponater et al., 2002] is run in spectral resolution T30 with 39

vertical layers. In the standard setup the IFSHAM model is run in spectral horizontal resolution T63 with a linear grid and 31 vertical layers defined as in the ECMWF Re-Analysis data - ERA-15 [Gibson et al., 1997].

Contrail properties in the IFSHAM model

A set of experiments has been performed with the IFSHAM model extended with the [Ponater et al., 2002] contrail parameterization in order to study contrail properties as they are determined by the IFSHAM model. The model is run in standard resolution, T63, 31 vertical layers and a time step of 30 minutes, and with climatological sea surface temperatures. As a measure for air traffic density determining the actual contrail coverage from the potentail coverage (F in equation 3.8) is, as in [Ponater et al., 2002], used the version 2 Deutsches Zentrum für Luft- und Raumfahrt aircraft emission data set, [Schmitt and Brunner, 1997], which represents air traffic density around 1992. Also as in [Ponater et al., 2002] the propulsion efficiency of the jet engine η (equation 3.2) is set to 0.3. Presented here is the annual mean of different contrail properties, based on one year long experiments. It might be argued that one year is too short a time period for representing the contrail properties, but a 10 year long experiment showed that the main characteristics discussed here are adequately described in one year long experiments.

Figure 3.1 shows the annual mean of the total contrail coverage. The contrail coverage has been adjusted using the tuning parameter γ (equation 3.8) to give a global mean of 0.13 % as in [Ponater et al., 2002]. It should be noted that figure 3.1 shows the coverage of all contrails whereas [Ponater et al., 2002] is showing the coverage of visible contrails. Contrails are defined as invisible if they are having an optical depth less than 0.02 in the visible part of the spectrum or if the coverage of natural cirrus clouds in the layer immediately above or below the contrail in a given layer is larger then 80 %. It should also be pointed out that [Ponater et al., 2002] is showing January means and July means, whereas annual means are shown here. Annual means from simulations similar to the simulations presented in [Ponater et al., 2002] can be found in [Marquart, 2003]. It is seen from figure 3.1 that there are distinct maxima over central Europe, eastern United States and the North Atlantic. The pattern of the contrail coverage is to a large degree determined by the air traffic density and the pattern compares well with the contrail coverage pattern shown in [Ponater et al., 2002] and [Marquart, 2003].

Figure 3.2 and 3.3 show the contrail coverage at model level 10 and 11, corresponding to approximately 210 hPa and 240 hPa respectively. As in [Ponater et al., 2002] the contrail coverage is generally largest at the lower level. This can be explained partly by air traffic density, and partly by the fact that level 10 is sometimes located in the stratosphere, where the humidity is too low for persistent contrail formation.

Figure 3.4, 3.5 and 3.6 shows the short wave forcing, the long wave forcing and the net radiative forcing, respectively, of contrails at the top of the atmosphere (TOA). The net forcing is determined as the sum of the short wave and the long wave forcing. Notice, that the unit is mW/m^2. The contrail forcing is determined as the difference between the fluxes obtained by calling the radiation scheme with and without contrails included in the cloud cover.

The short wave forcing is negative everywhere and the strongest forcing is seen over Europe and especially over the United States. The global mean of the short wave forcing is -3.0 mW/m^2; the [Ponater et al., 2002] estimate is -1.8 mW/m^2.

The long wave forcing is positive everywhere except for spots in the tropics with small negative values. Also the long wave forcing has maxima over the United States and Europe. The global mean

of the long wave forcing is 3.3 mW/m^2; the [Ponater et al., 2002] estimate is 2.0 mW/m^2. The long wave forcing as it is determined using the ECHAM4 model in [Ponater et al., 2002] does not have negative values anywhere, and the question is why it is seen with the IFSHAM model. An experiment was made in which the contrail radiative forcing was calculated, assuming that there were no natural clouds present. In this case the contrail long wave forcing was positive everywhere (result not shown), meaning that the spots with negative long wave forcing occur when there is an overlap between contrails and natural clouds. As explained in [Marquart and Mayer, 2002] negative contrail long wave forcing can occur if the effective emissivity approach (clouds are considered black with a modified cloud cover) is used in combination with the maximum-random cloud overlap assumption. Although the effective emissivity approach is not used in the RRTM long wave scheme, it could be suspected that in cases, where there are normal cirrus clouds in the layers next to the contrail layer and where the emissivity of the clouds is high, the maximum-random cloud overlap assumption could cause negative long wave contrail forcing. But further investigation is needed in order to clarify whether this is indeed the explanation for the negative long wave forcing values seen in figure 3.5.

The global mean of the net radiative forcing of contrails is 0.26 mW/m^2, very close to the [Ponater et al., 2002] estimate of 0.2 mW/m^2. Both the long wave and the short wave forcing is slightly stronger in the IFSHAM model compared to the ECHAM4 model, but the resulting net forcing is very similar in the two models, at least regarding the global mean. The geographical pattern of the net forcing is shown in figure 3.6. It is seen that although the global mean of the net forcing is positive there are large areas where the net forcing is negative with largest negative forcing over southern Europe. This result is quite different from the result obtained in [Ponater et al., 2002], where negative net forcing is seen too, but mainly in summer and north of 55 °N. Furthermore the long wave forcing of contrails in ECHAM4 has been investigated in a subsequent paper [Marquart and Mayer, 2002]. The conclusion of the paper is that the long wave forcing is underestimated in [Ponater et al., 2002], due to the effective emissivity approach used in combination with maximum-random overlap of clouds. To cure this problem, the long wave scheme of ECHAM4 is modified applying a modification introduced by [Raisanen, 1998]. A new estimate of the long wave forcing is then obtained, resulting in a global mean of 5.0 mW/m^2. The global mean of the net forcing is then estimated to 3.2 mW/m^2 and the geographical pattern is showing positive net forcing everywhere, [Marquart and Mayer, 2002]. There is therefore a clear disagreement between the results obtained with the IFSHAM model and the results obtained with the ECHAM4 model. Other studies [Fortuin et al., 1995] and [Meerkotter et al., 1999] indicate that negative net forcings only occur if the ice water content of the contrails are much larger than in these experiments. The question is now whether the long wave forcing is underestimated or the short wave forcing is overestimated in IFSHAM, or if in fact these simulations with the IFSHAM model could be reasonable. It should be emphasized, that the RRTM long wave scheme used in IFSHAM is not using the effective emissivity approach, but is treating cloud cover and emissivity seperately, meaning that the RRTM scheme is not suffering from the same problem as the long wave scheme used originally in ECHAM4.

The optical properties of the contrails are very important for the radiative impact of contrails. Two of these, optical depth and particle effective radius, are shown in figure 3.8 and 3.9 and the ice water path is shown in figure 3.7 in order to be able to compare with the results of [Ponater et al., 2002] and [Marquart, 2003], and see if differences in optical properties can explain the differences in the radiative forcing. Each of the figures are showing the annual, conditional mean at model level 10 and 11 for contrails with optical depth in the visible part of the spectrum (0.25-0.69 μm) larger than 0.02. The mean is conditional because it is only the average of the cases where contrails actually occur.

The ice water path (IWP) shown in figure 3.7 has largest values in the tropics where more water vapour is available for condensation in the contrails. The IWP at level 11 has values comparable to the results of [Ponater et al., 2002, Marquart, 2003], except for parts of the northern midlatitudes where the values are approximately a factor of two less in the IFSHAM simulation. At level 10 the values are comparable in the extratropics, but in the tropics the IFSHAM is showing a factor of two larger values. It should be noted, that [Ponater et al., 2002, Marquart, 2003] are showing results at vertical levels 200 hPa and 250 hPa, meaning that the two models are not compared at the exact same vertical levels.

The optical depth determined for the visible part of the spectrum is shown in figure 3.8. The geographical pattern of the optical depth is the same as the pattern of the IWP, again due to the higher water vapour content in the tropics. The optical depth in the IFSHAM model is generally a factor of two less everywhere than in the ECHAM4 model, except for north of 50 °N where the values are comparable.

The most remarkable difference between the two models is seen in the results for the particle effective radius, figure 3.9. In ECHAM4 the mean values of the effective radius lies in the interval between 12 and 13 μm, whereas in IFSHAM the values lies between 13 and 25 μm with a much larger north-south gradient.

In order to investigate whether the difference in effective radius can explain the difference in the net radiative forcing of the two models, the parameterization of effective radius in IFSHAM has been replaced by the parameterization used in ECHAM4. Results for optical depth and effective radius is shown in figure 3.10 and 3.11. It is seen that the values of the effective radius are now in the interval between 12 and 13 μm, as in the ECHAM4 model. But the values are slightly (app. 0.1 μm) less in large areas in the IFSHAM model. The values of the optical depth have approximately doubled in the areas where it was a factor of two less than the ECHAM4 results, with the original IFSHAM parameterization of effective radius. The optical depth in IFSHAM is now in good agreement with the optical depth in ECHAM4.

The question is now how this affects the radiative forcing of contrails in IFSHAM. In the experiment with the effective radius scheme in IFSHAM replaced by the ECHAM4 sheme the global mean of the short wave forcing is -3.8 mW/m^2. In the original version of IFSHAM the global mean is -3.0 mW/m^2. The global mean of the long wave forcing is changed from 3.3 mW/m^2 to 4.3 mW/m^2. The net radiative forcing is changed from 0.26 mW/m^2 to 0.44 mW/m^2. Both the long wave and the short wave forcing is increased with approximately 1 mW/m^2, the long wave forcing a little more than the short wave resulting in an increase of close to 0.2 mW/m^2 in the net forcing. The long wave forcing is approaching the [Marquart and Mayer, 2002] estimate of 5 mW/m^2, while the short wave forcing is now 2 mW/m^2 larger than the [Marquart and Mayer, 2002] estimate and the net forcing is still almost a factor of 10 less than the [Marquart and Mayer, 2002] estimate. The geographical pattern of the net forcing is shown in figure 3.12, and it is seen that there are still large areas with negative net forcing, the pattern in figure 3.12 being very similar to the pattern of the net forcing obtained with the original IFSHAM, figure 3.6. The different parameterizations of the effective radius can therefore not explain the main differences in contrail radiative forcing between IFSHAM and ECHAM4.

The contrail coverage of [Ponater et al., 2002] has been adjusted to observed contrail coverage for the east Atlantic and western Europe area as determined in [Bakan et al., 1994]. Newer observations, [Meyer et al., 2001], indicate that the [Bakan et al., 1994] contrail cover may be a factor of two too large. Therefore some sensitivity experiments have been performed with a contrail coverage having a global mean half the value of the global mean in the experiments described above. Table 3.1

Experiment	Effective radius param.	Optical depth	SW forcing	LW forcing	Net forcing
1	IFSHAM	variable	-1.4	1.5	0.1
2	ECHAM4	variable	-1.8	2.0	0.2
3	12 μm	0.1	-3.4	5.3	1.9
4	12 μm	0.3	-7.7	14.5	6.7
5	12 μm	0.5	-11.4	22.0	10.6

Table 3.1: Global, annual mean of contrail radiative forcing (unit: mW/m^2) for 5 sensitivity experiments. Global mean of contrail coverage is 0.067 %. SW: short wave, LW: long wave

contains the results of the sensitivity experiments regarding radiative forcing of the contrails.

Experiment 1 and 2 are similar to the two experiments described in detail above. Experiment 1 is performed with the standard version of IFSHAM and experiment 2 with the version of IFSHAM where the effective radius parameterization has been replaced by the one used in ECHAM4. The only difference to the above described experiments is that the contrail coverage is reduced by a factor of two. From table 3.1 it is seen that this reduction in contrail coverage implies a reduction by a factor of two in the radiative forcings. Experiment 3 to 5 are performed using constant values for the effective radius (12 μm) and for the optical depth (0.1, 0.3 and 0.5 in the three experiments respectively) in the visible part of the spectrum. The optical depth of contrails as determined by IFSHAM is much smaller in the extratropics than these fixed values. Typically, the optical depth of visible contrails over Europe for example is 0.02-0.05. Using these relatively high, constant values for the optical depth results in a considerable increase in short wave but especially in the long wave forcing, and therefore also the net forcing is increased substantially. These experiments are not exactly comparable to similar experiments in [Ponater et al., 2002] and [IPCC, 1999], but point in the same direction, and the net forcing in these experiments is one to two orders of magnitude larger than the net forcing determined in experiment 1 and 2. Figure 3.13 shows the geografical distribution of the net radiative forcing from experiment 3. It is seen that except in the tropics the net radiative forcing is positive everywhere with maxima over Europe and the United States, a pattern similar to the pattern shown in [IPCC, 1999], but in contrast to the pattern shown in figure 3.6.

It can be concluded from these experiments that the main difference between the radiative forcing as determined by the IFSHAM model and the ECHAM4 model is seen when the models are allowing for contrails having variable optical depth with relatively small values in the extratropics, meaning that the response of the radiation schemes in the two models to optically very thin ice clouds are quite different.

It is seen from these experiments that optical depth is a key parameter in determining the radiative forcing of contrails and that also the effective radius have some impact. There is a huge uncertainty in the determination of these two parameters, both in observations and in model simulations. To investigate further the magnitude and geographical distribution of contrail optical depth and effective radius microphysical simulations with the MPC model have been performed and are described in the following chapter.

The nudging technique

All general circulation models exhibit certain long term systematic errors when compared to observations. One way to address the impact of these systematic errors on contrail behaviour is to use the nudging technique, [Jeuken et al., 1996]. When using this technique the model is forced

towards a reference data set, and when the reference data set represents observed data the systematic errors of the model are minimized, because in each time step the model is following closely the observed values of the prognostic variables. Nudging is a simple 4-dimensional assimilation of the reference data, where the prognostic model variables are relaxed towards the reference data:

$$\Psi(t+\Delta t) = \Psi^*(t+\Delta t) + \Delta t \frac{\Psi^{REF}(t+\Delta t) - \Psi^*(t+\Delta t)}{\tau} \tag{3.9}$$

The upper index $*$ indicates the preliminary prognostic variable just before nudging and the upper index REF denotes the reference variable the model is relaxed towards. Δt is the length of the time step used in the model and τ is the relaxation time. The ECMWF Re-Analysis data (ERA-15) [Gibson et al., 1997] are used as the reference data towards which the model is relaxed. These data are available every 6 hours in T106, L31 resolution. In order to use them for nudging they have to be truncated to the horizontal resolution used in the IFSHAM model (T63), and interpolated in the vertical to the orography-adjusted hybrid levels. As the relaxation towards the reference data is done at every time step (in this case every 30 minutes) a cubic spline interpolation is used to obtain reference data at intermediate times. In practical use of the nudging technique the relaxation time τ has to be chosen carefully. If τ is too small noise and spin-up problems play an important role, but if τ is too large the model is not following the reference data set closely. The variables assimilated were temperature, vorticity, divergence, logarithm of surface pressure, and the variables were nudged in spectral space. The τ used was not the same for all the variables. The actual values were: 24h for temperature, 6h for vorticity, 48h for divergence and 24h for logarithm of surface pressure. The atmospheric humidity field was not nudged. The reason for this is that processes related to humidity can act on a time scale smaller than 6 hours (the temporal resolution of the reference data set in this case) through threshold processes like condensation and deep convection. To avoid moisture spin-up problems it therefore makes more sense to let the model develop its own humidity field. This is especially important in the tropics where convection plays a large role. For a description of how the values for τ were determined see [Guldberg et al., 2004]

Impact of systematic errors on contrail behaviour in IFSHAM

In order to study the impact of systematic errors on contrail behaviour two sets of simulations have been performed with the IFSHAM model. In the first set - the control simulations - the model is forced with observed sea surface temperatures for ten winter seasons and 10 summer seasons in the period covered by the ERA-15 data set (1979-1993). In the second set - the nudged simulations - the model is run in nudged mode and the model is relaxed towards observed data for the same 10 winter and summer seasons as in the control simulations. Also observed sea surface temperatures are used in the nudged simulations. In the following averages over the 10 winter and the 10 summer simulations are shown and compared for the two sets of simulations. The contrail cover in these simulations are determined using the same calibration factor γ as used in the first experiment described in this report, giving an annual mean contrail cover of 0.13 % as in [Ponater et al., 2002] for all contrails.

The IFSHAM model as compared to the ERA-15 data is generally too cold in most of the atmosphere in both summer and winter with the largest cold biases in the extratropical upper troposphere and lower stratosphere - meaning at altitudes where most airplanes fly. Figure 3.14 is showing the difference between the temperature at model level 10 of the control simulations and the nudged simulations for the winter (DJF) and the summer (JJA) season, and 3.15 is showing the difference for model level 11. As the nudged simulations are following the ERA-15 data closely the

differences in figure 3.14 and 3.15 are in very good agreement with the systematic errors of the model determined as the difference between the control simulations and the ERA-15 data. It is seen that in winter the IFSHAM model is too cold almost everywhere on both levels. The largest biases are seen at Antarctica and in the northern Pacific. In the summer season the model is too warm at Antarctica and too cold almost elsewhere. The largest cold biases are seen at northern high latitudes. The biases in the tropics are generally relatively small.

Figure 3.16 and 3.17 are equivalent to figure 3.14 and 3.15, but showing the relative humidity with respect to ice. A general pattern is that the relative humidity in IFSHAM is too low a high latitudes and in the tropics whereas it is too high a midlatitudes (with some exceptions). It should be noted that humidity is not nudged in these experiments, so the humidity in the nudged simulations is determined by the model based on close to observed values of the other prognostic variables.

Figure 3.18 is showing the ratio between the control and the nudged simulations of the total contrail coverage. It is seen that the differences between the two model simulations to a large degree follow the pattern of the differences of the relative humidity, indicating that the relative humidity is likely the determining factor for these differences. But in most areas the differences between the two model simulations are relatively small and the global mean of the contrail coverage is almost unchanged.

Figure 3.19 and 3.20 show the ratio between the control and the nudged simulations of ice water path and the optical depth, respectively, at level 11. Figure 3.21 show the differences between the control and the nudged simulations for the effective radius at level 11. The differences in ice water path between the control and the nudged simulations are rather small, but there is a tendency of too large values in the tropics and too small values in the extratropics in the control simulations. As the effective radius and the optical depth are determined from the ice water path, the same tendency is seen for the effective radius and the optical depth. Results for level 10 are not shown, as the general picture is the same as for level 11.

The main question is how the model biases affect the radiative forcing of contrails in the IFSHAM model. Figure 3.22 and 3.23 show the changes in short wave and long wave forcing. As the sign of the short wave forcing is negative positive values in the difference plot in figure 3.22 mean that the magnitude of the forcing is too low in the control simulations and this is the case almost everywhere in winter. In summer the magnitude of the short wave forcing is too low over the northern part of the United States, the north Atlantic fligt corridor and northen Europe. In the southern part of the United States and southern Europe the magnitude of the forcing is too large in the control simulations. In global mean the magnitude of the short wave forcing is increased by 0.4 mW/m^2 in both summer and winter when the model is nudged.

As seen in figure 3.23 the long wave forcing in the control simulations is too weak almost everywhere in winter and too weak, respectively too strong in the areas where the short wave forcing is too weak, respectively too strong in summer. The global mean of the long wave forcing is increased by 0.6 mW/m^2, when the model is nudged.

Comparing figure 3.22 and 3.23 with the figures 3.19, 3.20 and 3.21 it is seen that the pattern of changes in the radiative forcings follows closely the pattern of changes of the ice water path and the optical properties, meaning it is likely that the changes in radiative forcings can be explained by the changes in these properties.

The net radiative forcing for the control and the nudged simulations is shown for winter in figure 3.24 and for summer in figure 3.25. The net forcing in winter is approximately 25 % of the forcing in summer. The global mean of the net forcing is increased by 0.2 mW/m^2 in both winter and summer

when the model is nudged. In winter the net forcing is increased by a factor of 4 from 0.07 to 0.3 mW/m^2. In summer the net forcing is changed from 0.8 to 1.0 mW/m^2. Although the magnitude of the net forcing is changed the pattern of the forcing is to a large degree unchanged. It should be noticed that the negative net forcing over the United States is seen only in winter, not in summer.

As shown here the systematic errors have some impact on the radiavtive forcing of contrails - the increase in the magnitude of the short and long wave forcing is 10-20 % when the model is nudged as compared to the free simulation with the model. But the short wave and the long wave forcing is still to a high degree cancelling each other resulting in a small net forcing an order of magnitude less than obtained by [Marquart and Mayer, 2002], and the pattern of the net forcing having areas with negative values are not changed when the model is nudged.

[Marquart et al., 2003] has studied the impact of systematic errors on contrail coverage by off-line simulations, but the systematic errors of the ECHAM4 model, especially regarding relative humidity, are somewhat different from the systematic errors of the IFSHAM model, and therefore the results are not directly comparable.

Conclusions

The contrail parameterization of [Ponater et al., 2002] has been implemented in the IFSHAM model and the contrail properties have been analyzed according to model dependency and impact of model systematic errors.

The magnitude of the contrail short wave forcing is larger than obtained by [Marquart and Mayer, 2002] and the contrail long wave forcing smaller. The resulting global mean of the contrail net forcing is an order of magnitude less than the [Marquart and Mayer, 2002] estimate. The net forcing shows areas over Europe and the United States with negative values. This is not seen by [Marquart and Mayer, 2002]. In their simulations the net forcing is positive everywhere.

Optical properties are important for the radiative impact of contrails. The magnitude and geographical distribution of the effective radius is quite different in IFSHAM and ECHAM4. Replacing the effective radius parameterization of IFSHAM with the one from ECHAM4 has some impact on the radiative forcing, but does not explain the main differences between IFSHAM and ECHAM4.

IFSHAM experiments with fixed increased values of the optical depth at 0.1, 0.3 and 0.5 show a significant change in the radiative forcing of the contrails, resulting in net forcings in better agreement with other estimates and with positive net forcing everywhere (except for negative spots in the tropics). But it is a question how realistic these values for the optical depth are.

The impact of the systematic errors of the model has been studied using the nudging technique. The systematic errors are causing a 10-20 % too low estimate of the short and long wave forcings. The net forcing is 75 % too low in winter and 20 % too low in summer in the control model compared to the nudged version of the model. But the geographical distribution of the net forcing is unchanged.

In order to understand the differences in radiative forcing of contrails in the two models a detailed investigation of the differences in the radiation parameterizations for both long and short wave used in the two models is needed. Also an analysis of the many different parameterizations of optical properties available could be of importance for the understanding the differnces seen with these two models.

The [Ponater et al., 2002] parameterization of contrails is only representing line-shaped contrails and not cirrus clouds developed from these contrails. The contrail derived cirrus is likely to have a much larger radiative impact than the line-shaped contrails. DMI will participate in an EU-project, QUANTIFY, starting in 2005 and one of the obligations of DMI is to implement a parameterization scheme in IFSHAM, describing the development of line-shaped contrails into cirrus clouds. Furthermore nudging experiments with IFSHAM in high resolution, T159 and 60 vertical layers, will be performed and compared with analyses of satellite images. Especially the very high vertical resolution is likely important for the representation of contrails and contrail derived cirrus.

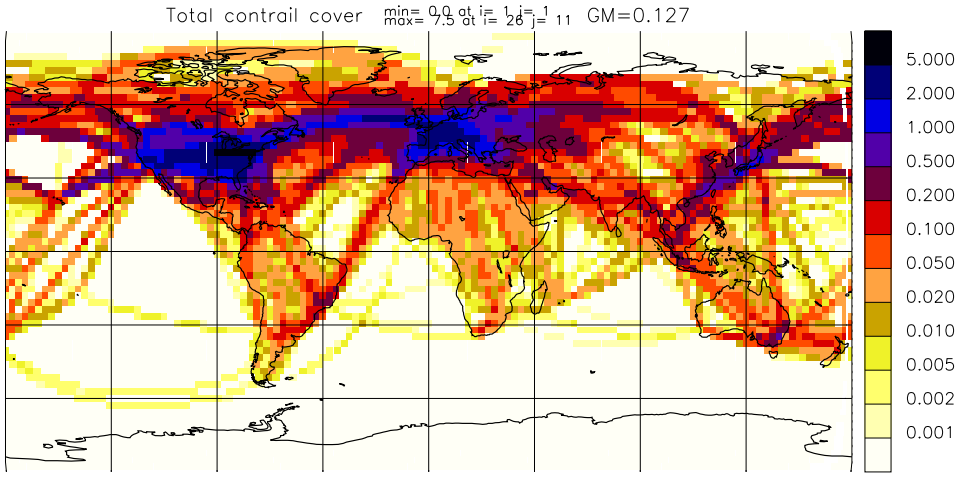

Figure 3.1: Annual mean of total contrail coverage (%)

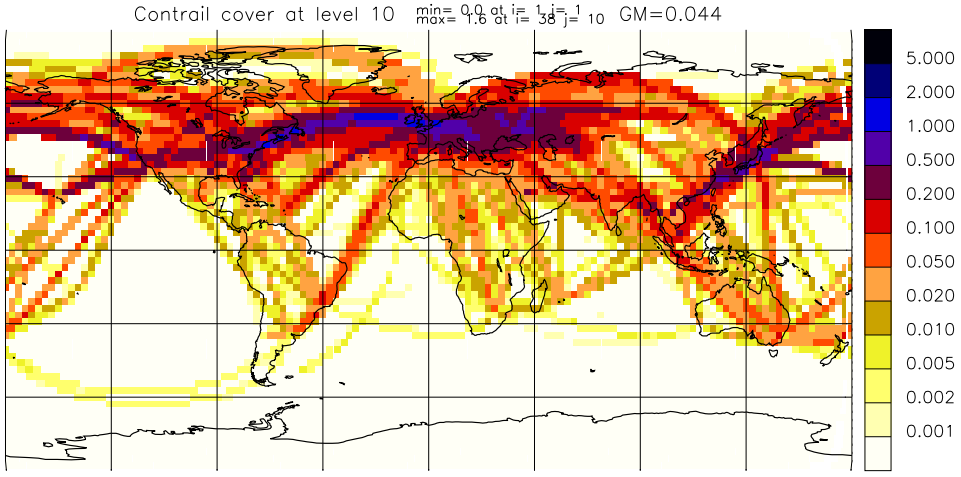

Figure 3.2: Annual mean of contrail coverage (%) at model level 10 (∼ 210 hPa)

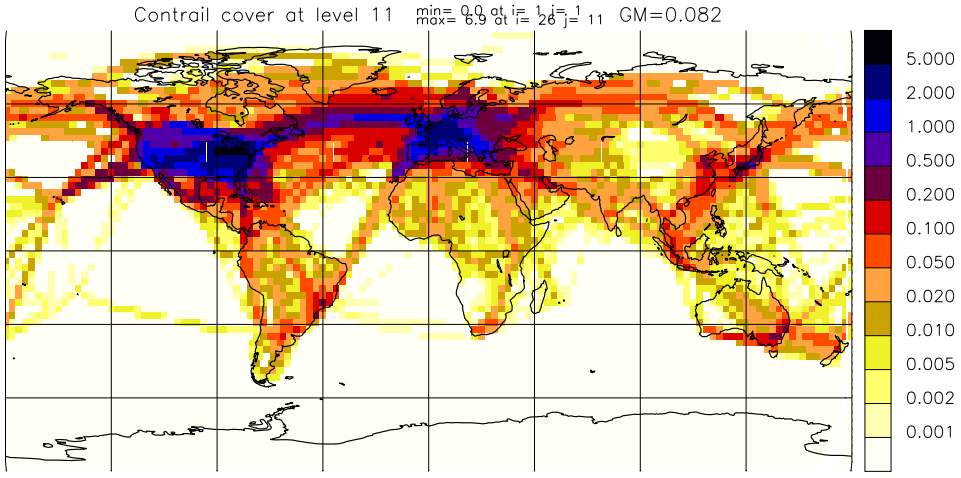

Figure 3.3: Annual mean of contrail coverage (%) at model level 11 (∼ 240 hPa)

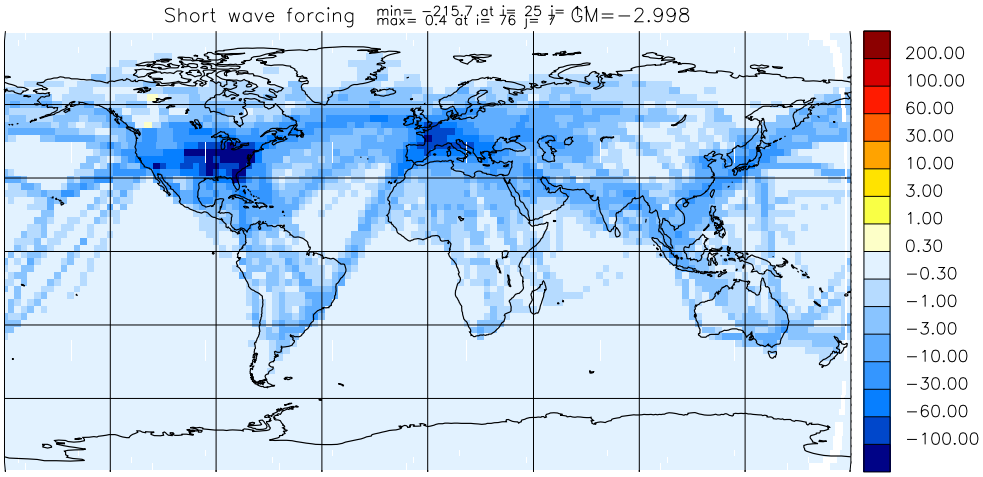

Figure 3.4: Annual mean of contrail short wave forcing at TOA (mW/m^2)

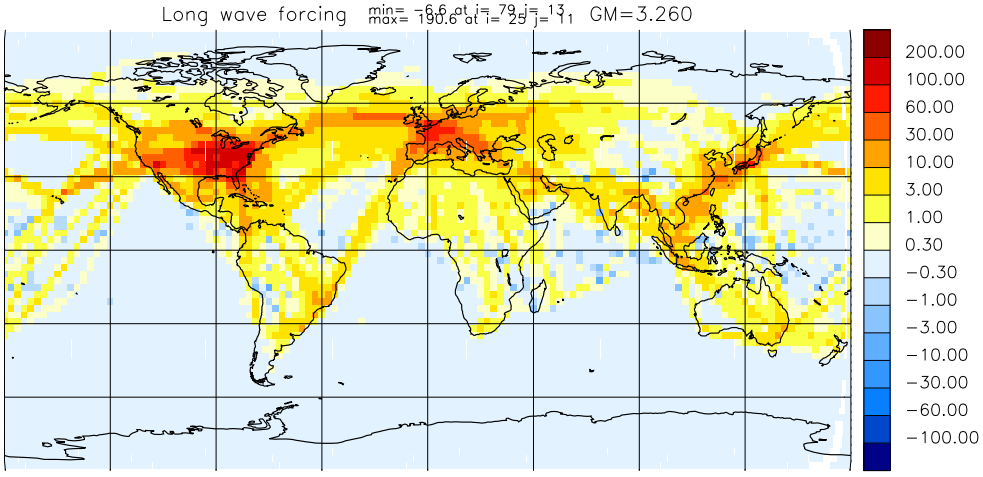

Figure 3.5: Annual mean of contrail long wave forcing at TOA (mW/m^2)

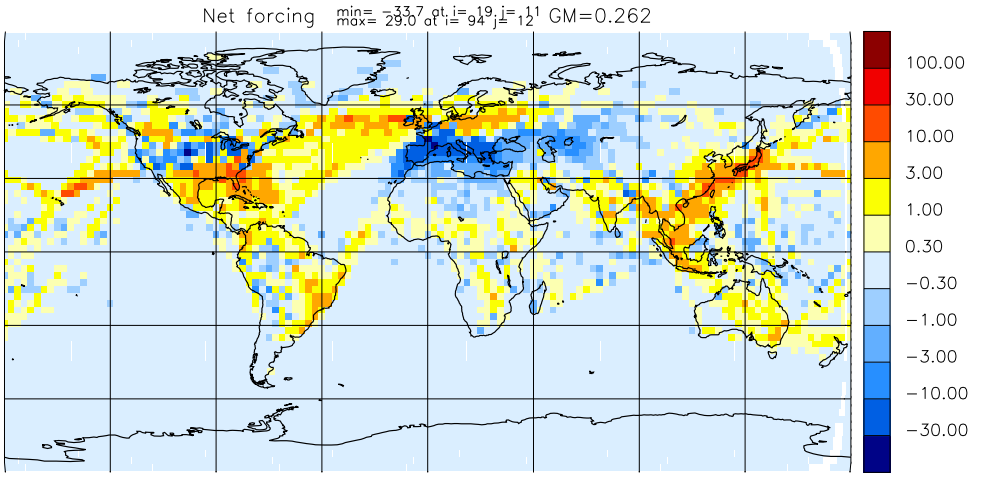

Figure 3.6: Annual mean of contrail net forcing at TOA (mW/m^2)

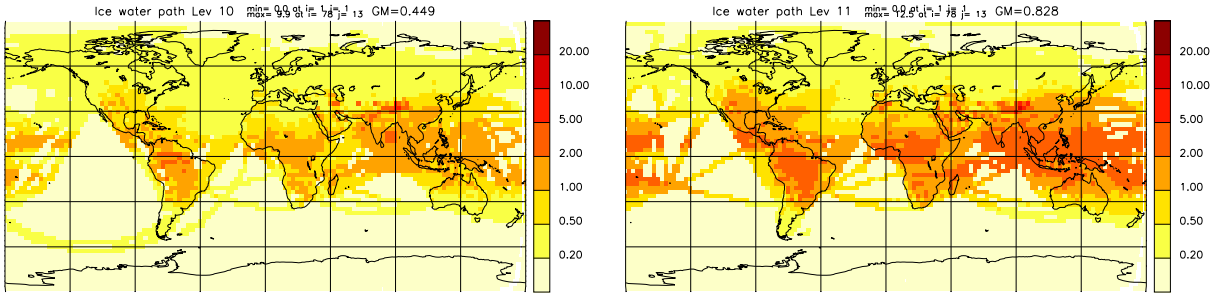

Figure 3.7: Annual, conditional mean of the ice water path for contrails at level 10 (left) and level 11 (right) (g/m^2)

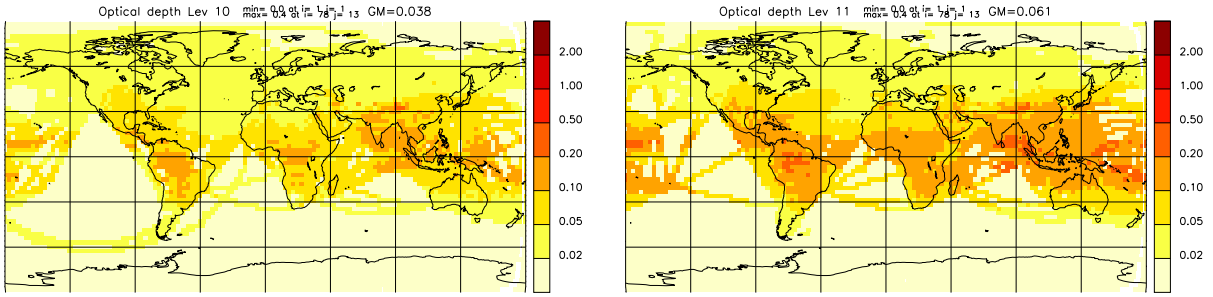

Figure 3.8: Annual, conditional mean of the optical depth for contrails at level 10 (left) and level 11 (right).

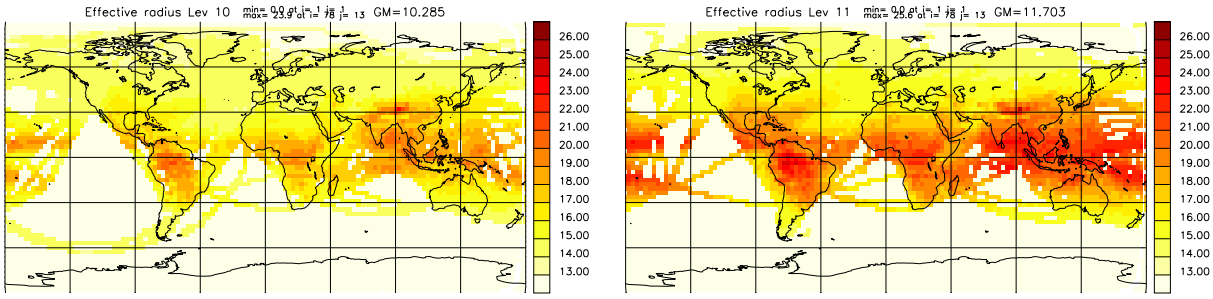

Figure 3.9: Annual, conditional mean of the effective radius for contrails at level 10 (right) and level 11 (left) (μm).

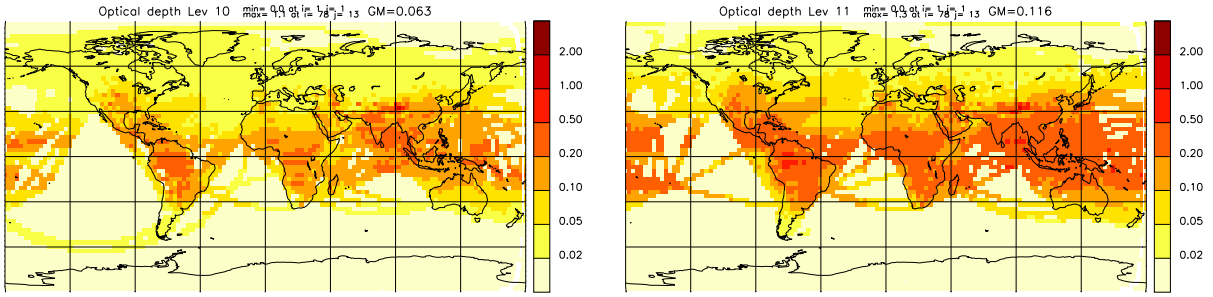

Figure 3.10: Annual, conditional mean of the optical depth for contrails at level 10 (left) and level 11 (right). - ECHAM4 effective radius

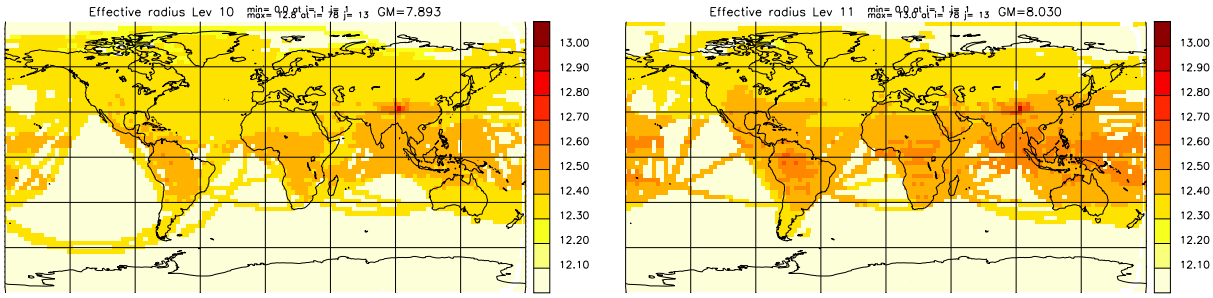

Figure 3.11: Annual, conditional mean of the effective radius for contrails at level 10 (right) and level 11 (left) (μm). - ECHAM4 effective radius

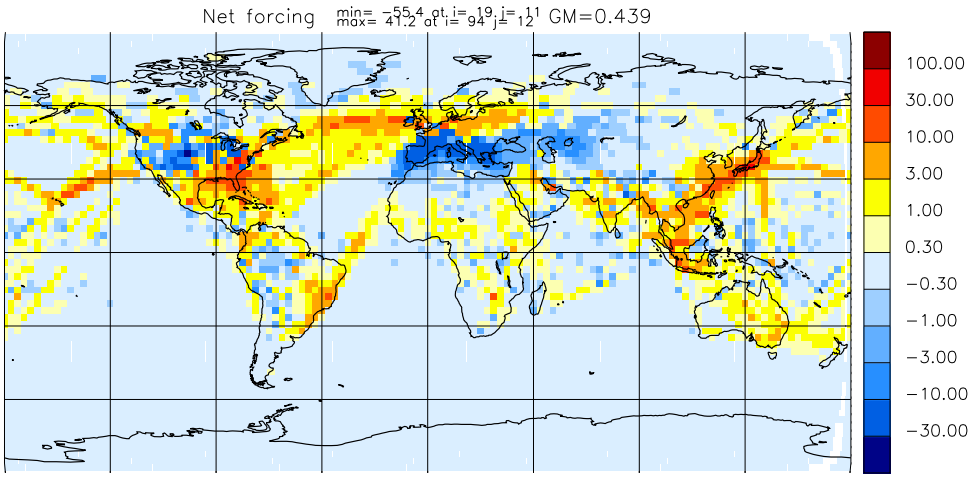

Figure 3.12: Annual mean of contrail net forcing at TOA (mW/m^2) - ECHAM4 effective radius

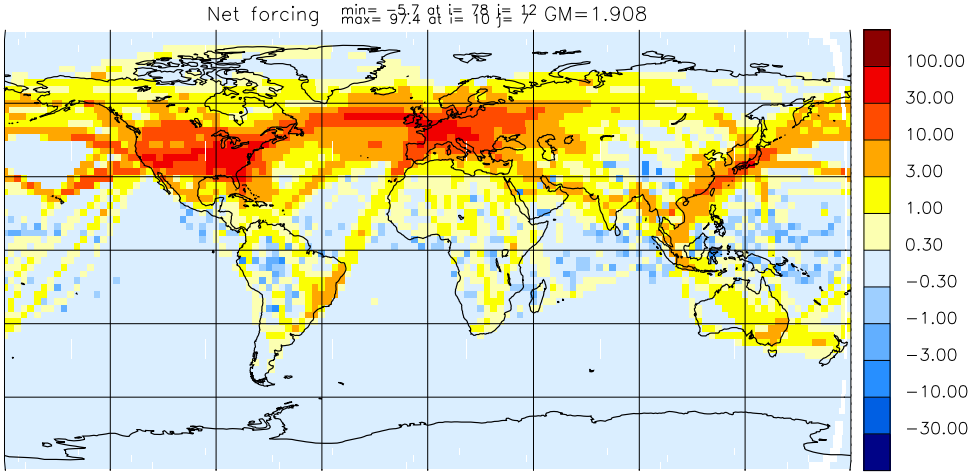

Figure 3.13: Annual mean of contrail net forcing at TOA (mW/m^2) - Optical depth: 0.1

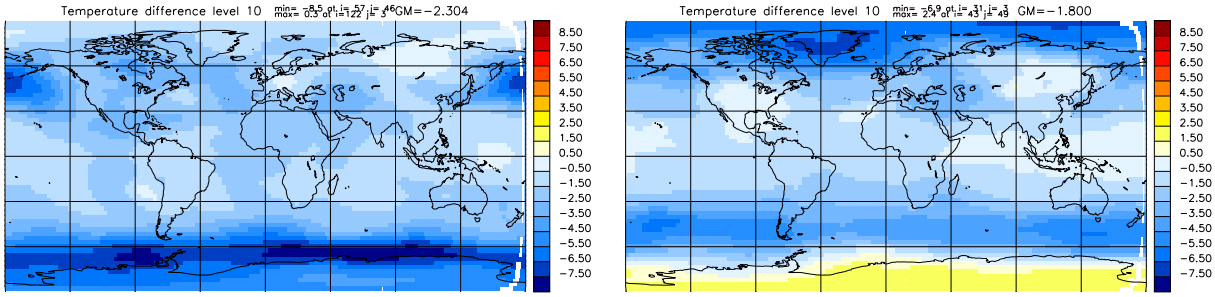

Figure 3.14: Ten-year mean differences of temperature between control and nudged simulations at level 10 for DJF (left) and JJA (right) (K)

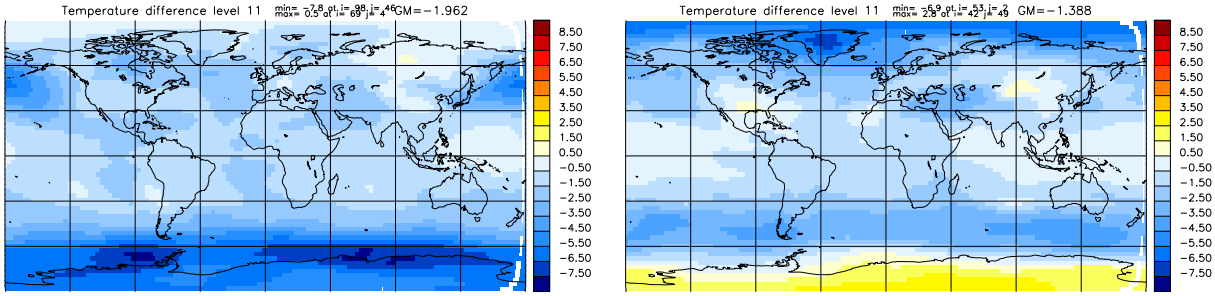

Figure 3.15: Ten-year mean differences of temperature between control and nudged simulations at level 11 for DJF (left) and JJA (right) (K)

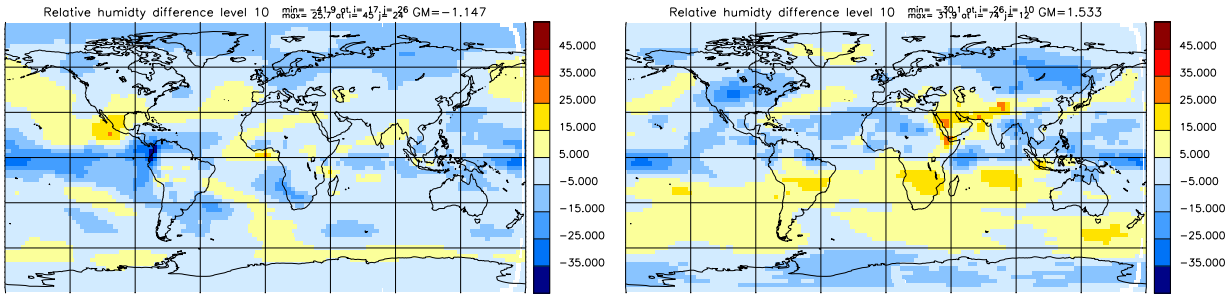

Figure 3.16: Ten-year mean differences of relative humidity with respect to ice between control and nudged simulations at level 10 for DJF (left) and JJA (right) (%)

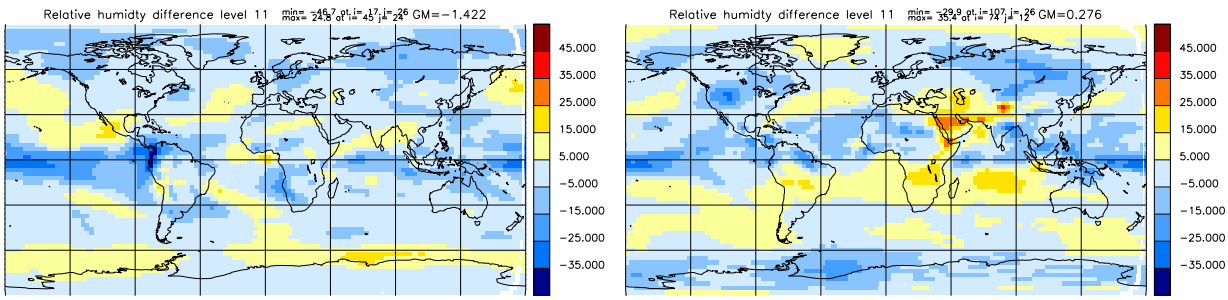

Figure 3.17: Ten-year mean differences of relative humidity with respect to ice between control and nudged simulations at level 11 for DJF (left) and JJA (right) (%)

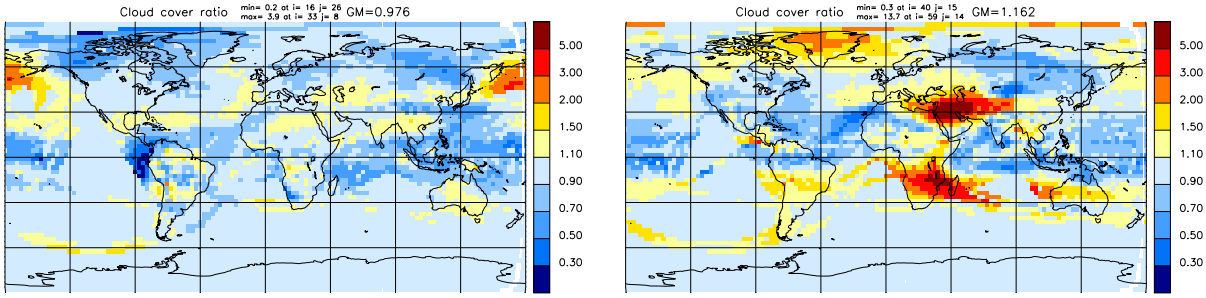

Figure 3.18: Ratio between control and nudged simulations of ten-year mean of total contrail coverage for DJF (left) and JJA (right)

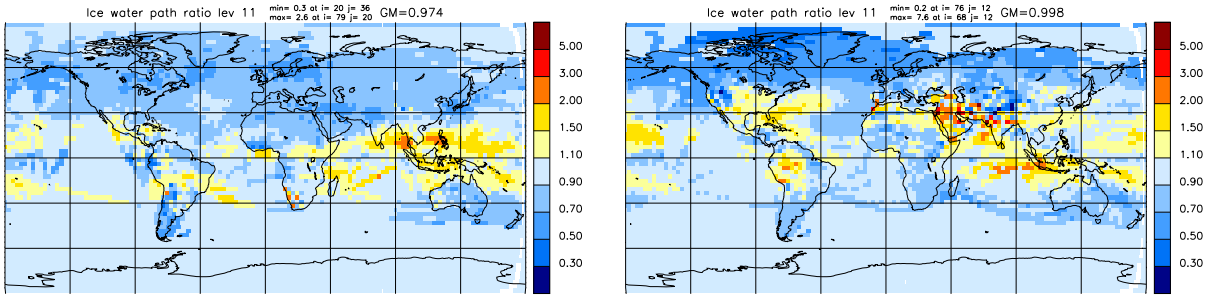

Figure 3.19: Ratio between control and nudged simulations of ten-year mean of ice water path at level 11 for DJF (left) and JJA (right)

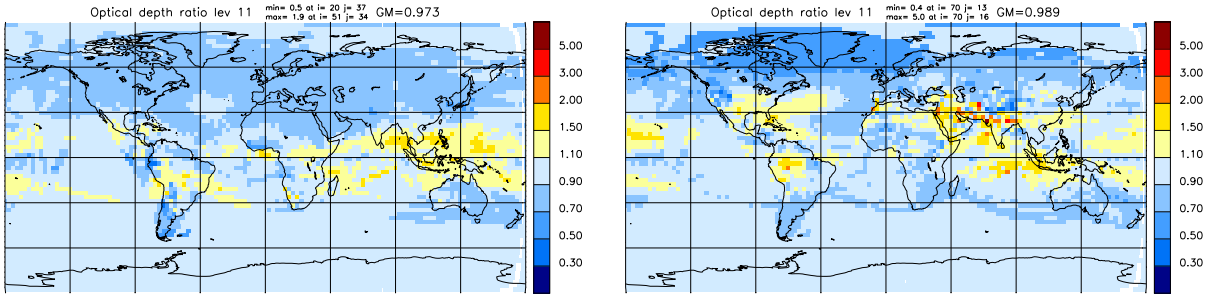

Figure 3.20: Ratio between control and nudged simulations of ten-year mean of optical depth at level 11 for DJF (left) and JJA (right)

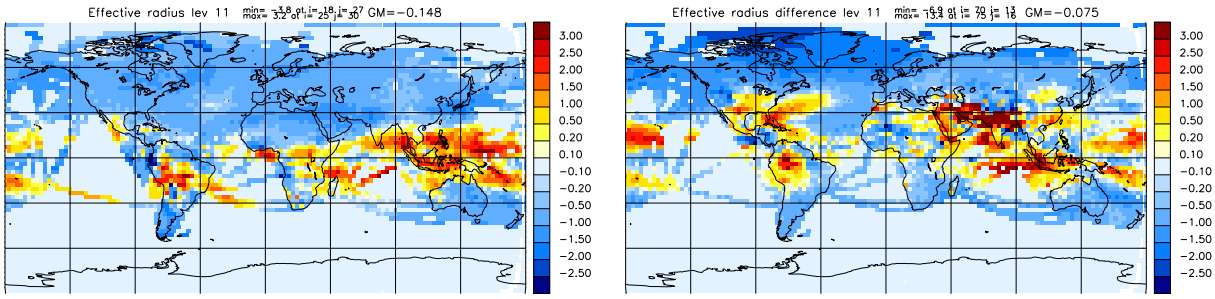

Figure 3.21: Ten-year mean differences of effective radius between control and nudged simulations at level 11 for DJF (left) and JJA (right) (μm)

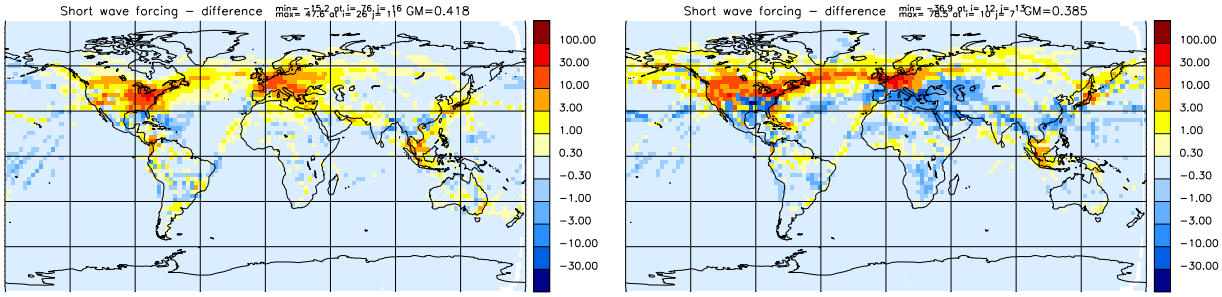

Figure 3.22: Ten-year mean differences of short wave radiative forcing between control and nudged simulations for DJF (left) and JJA (right) (mW/m^2)

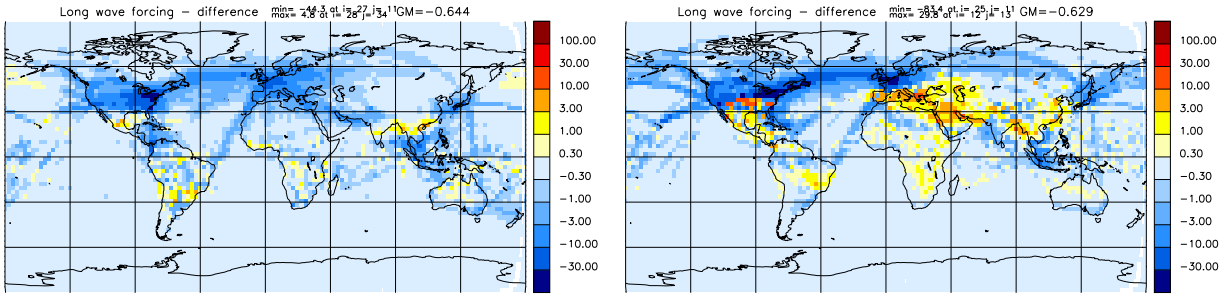

Figure 3.23: Ten-year mean differences of long wave radiative forcing between control and nudged simulations for DJF (left) and JJA (right) (mW/m^2)

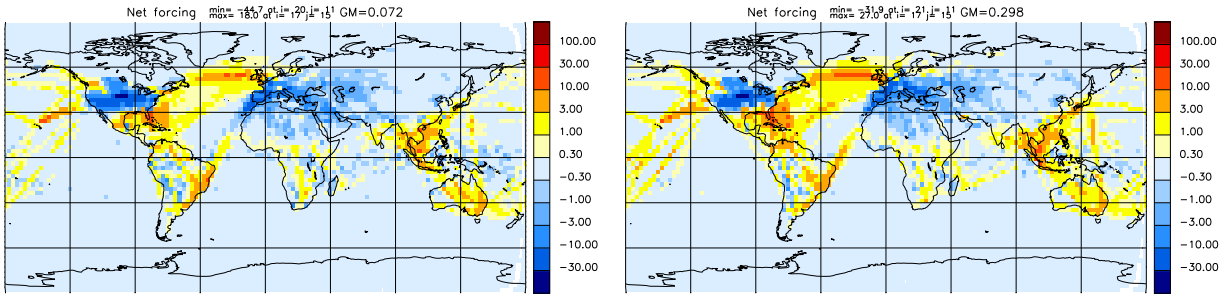

Figure 3.24: Ten-year mean of net radiative forcing for control (left) and nudged simulations (right) for DJF (mW/m^2)

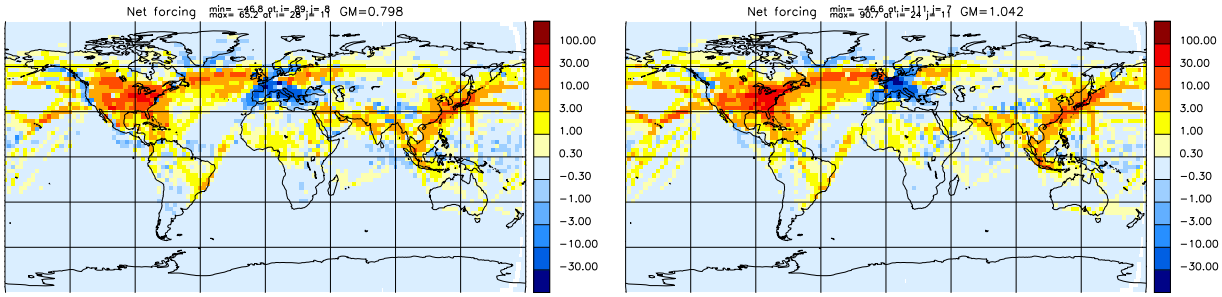

Figure 3.25: Ten-year mean of net radiative forcing for control (left) and nudged simulations (right) for JJA (mW/m^2)

Microphysical simulations of spreading contrails

Motivation

The climatological impact of contrails and contrail-derived cirrus clouds depends on microphysical properties of these types of clouds. That is, the size distribution and shapes of the particles, the ice water content and of course the spatial formation of the clouds. All these characteristics change in time as a cloud evolves, and they depend on the local environment. The growth of airplane contrails into cirrus clouds is mainly controlled by initial humidity, wind shear, temperature and radiative heating caused by interaction of ice particles with infrared radiation.

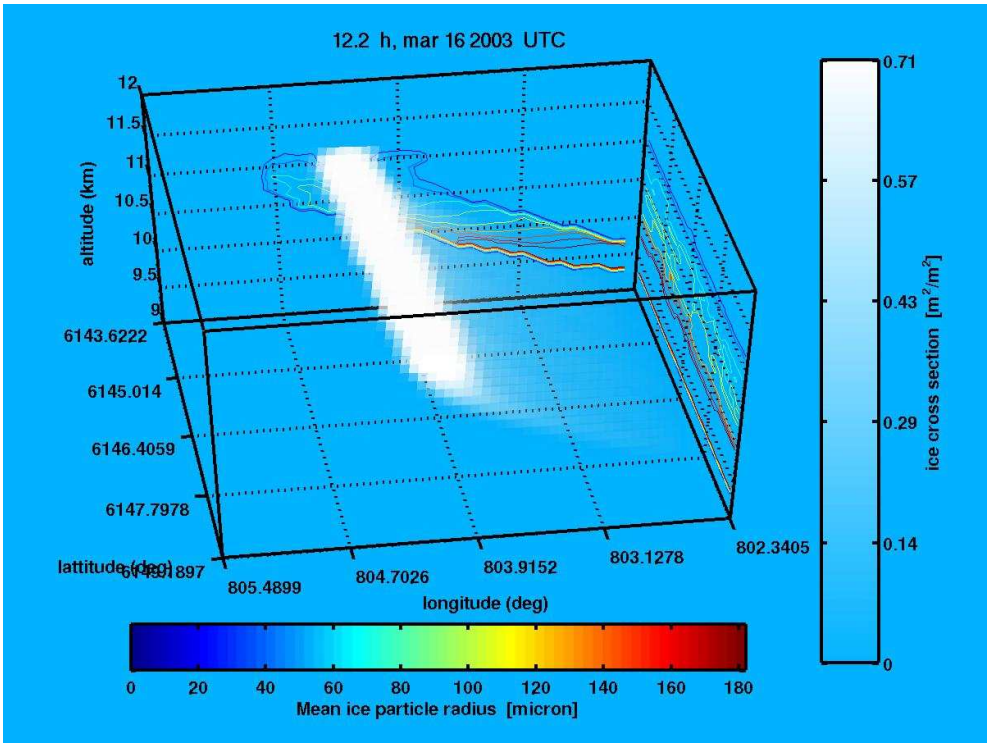

Figure 4.1: Example of a MPC contrail simulation (afternoon March 16 2003, eastern Denmark). Wind, temperature and pressure was taken from ECMWF (European Centre for Medium-Range Weather Forecast) in this simulation, while the humidity was initiated with values from local radio soundings. Looking through the cloud one sees the integrated cross section area, which gives a good impression of the physical distribution of the cloud. From [Nielsen, 2004].

Ground LIDAR observations [Larchevêque et al., 2002, Del Guasta and Niranjan, 2001] and airplane observations [Jensen et al., 1998, Heymsfield et al., 1998, Lawson et al., 1998, Schröder et al., 2000] of developing contrails provides information about contrail-cirrus optical properties, humidity and particle distributions. The drawback of these observations is that it is hard to track a cloud history, since observations are restricted to a vertical profile at a given location or a single point at a given time. In order to establish a relation between the cloud properties and the conditions at the point where the cloud was created, it is necessary to follow the history of a specific cirrus cloud. This can be done by satellite observations. Observations of contrail cirrus by satellite images has been investigated by [Mannstein and Schumann, 2004, Minnis et al., 1998]. A problem with satellite observations is to separate contrails from ordinary cirrus clouds as they become more and more similar during the lifetime of a contrail. Furthermore satellite observations does not provide detailed information of local humidity in the contrail and its surroundings.

It is therefore desirable to perform detailed cloud resolving and microphysical modeling of contrails in order to get information about their temporal and spatial development, and their microphysical properties. This has been done for a special case by [Jensen et al., 1998] in the SUCCESS campaign, and here the thread off that study is taken up with the purpose of comparing microphysical simulations to the global climate model IFSHAM.

Simulation method

The MicroPhysical Cirrus (MPC) model is an integrated model, developed at DMI, which combines a well tested microphysical box-model with a quite accurate 3-D advection scheme. The microphysical kernel was originally developed for simulations of PSC clouds ([Larsen, 2000]), and as a consequence the MPC-model may be applied on PSC-clouds as well as cirrus clouds. The dynamical variables of the model are gas-phase mixing ratios of water and HNO3, size-distributions of 4 different particle types, (supercooled ternary solutions, sulphuric acid tetrahydrate, nitric acid trihydrate and ice) and in-particle weight fractions of condensed phase constituents. The model includes nucleation and deposition-processes and detailed sedimentation calculation on each size bin. Wind transport, sedimentation and parts of the particle growth processes are calculated by the Walcek-algorithm [Walcek, 2000].

The model is linked with optical routines enabling extinction coefficients and backscattering ratios to be calculated. The software is flexible, in the sense that a lot of parameters is specified as input, and therefore it is easy to change e.g. dimensions, location, processes, initialization, output etc. The model is running off line, meaning that it does not include dynamical feedback from cloud-processes; the wind/temperature and pressure history has to be given beforehand. Modules has been written facilitating this to be done in several ways, e.g. by loading ECMWF fields into the model, generating fields from radio soundings (as in figure 4.1), or by constructing artificial fields for theoretical analysis (as in figure 4.4).

Simulations aims and setup

The purpose of the simulations described here is to compare the MPC-models predictions of contrail-cirrus cloud effective radius and optical depth, with the corresponding parameters of the IFSHAM model. To establish this comparison MPC simulations are done in an environment resembling the wintertime conditions in North Atlantic flight corridor. Information about these conditions cannot be retrieved from ECMWF, since the ECMWF relative humidity with respect to ice is restricted to below 100 %. Instead UTLS profiles are retrieved from radio soundings in (and near) the North Atlantic. The reason for choosing the North Atlantic region is that it is an area with relatively large and homogeneous flight load.

Analysis of radio soundings

Radio soundings from 7 different stations around the North Atlantic were retrieved from the Wyoming database [UWYO, 2004]. The chosen data-set includes all soundings from February 2004. In figure 4.2 profiles of the saturation ratio with respect to ice, S_i, are plotted for all stations, in the cases where supersaturation occurs somewhere between 8 and 12 km altitude. An autocorrelation function is formed from the parts of profiles exceeding $S_i = 1$, and this function is used to calculate a typical length depth Δz of a supersaturated region below an arbitrary positioned contrail. It should be noted that Δz is probably an underestimate for two reasons: First, the supersaturated regions has a tendency to occur in the lower part of the flight corridor, causing a bigger likelihood for the contrail to appear in the upper part of the supersaturated region, and secondly the RS80 humicap radiosonde, which presumably has been used, are known to underestimate humidities near the tropopause

[Wang et al., 2003].

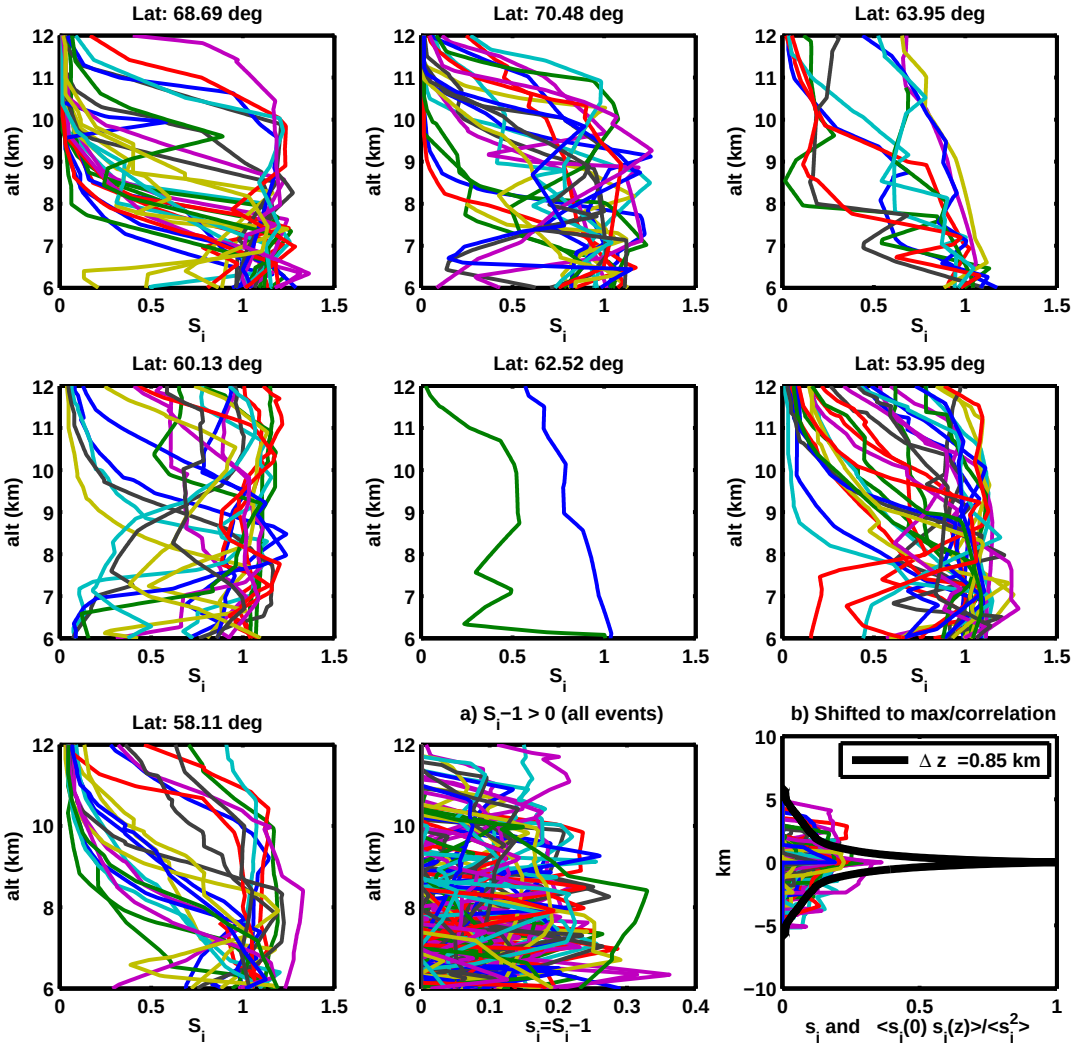

Figure 4.2: Saturation ratio profiles (with respect to ice) for 7 radiosonde stations in the North Atlantic and surroundings, all from February 2004 [UWYO, 2004], no corrections has been made. Only soundings where contrails potentially could form, i.e. soundings with $S_i > 1$ at some level, are shown. The last plots shows (a) all observations of $S_i - 1 > 0$, and (b) the same, but centered at maximum S_i. The black curve in (b) is the normalized vertical autocorrelation of $s_i = S_i - 1 > 0$; $c(z) = \langle s_i(0)s_i(z)\rangle / \langle s_i^2\rangle$. This correlation function is integrated in order to extract a characteristic geometrical depth; $\Delta z = \int_0^\infty c(z)dz$ of a supersaturated region.

In figure 4.2 the profiles with supersaturation are shown for 7 stations. From the autocorrelation function it is estimated that the typical depth of a supersaturated region below a contrail is 0.85 km. Given the arbitrariness of the radiosonde positions, and the systematic differences between stations, this number can only serve to approximate a typical (half) thickness.

The wind shear, illustrated in figure 4.3 has a somewhat lower persistence length. The horizontal wind has rather large vertical correlation length (several km's -not shown in figure). However the relevant feature for the simulations is the wind-shear which shows a correlation depth of only 0.2-0.3 km. This length is calculated from the auto correlation functions $C_{[u,v]}(z) = \langle \delta\frac{d[u,v]}{dz}(0)\delta\frac{d[u,v]}{dz}(z)\rangle$.

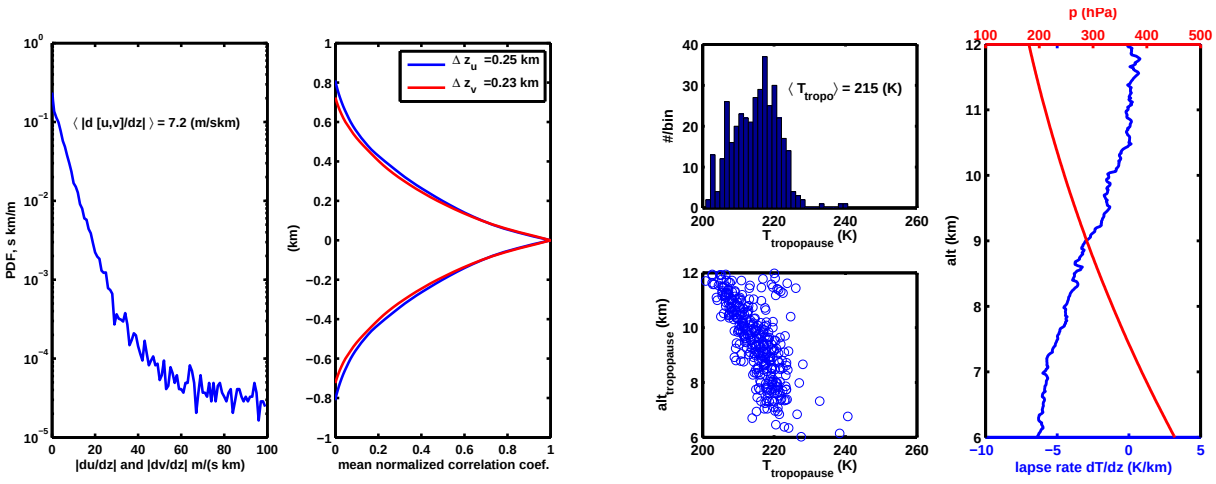

Figure 4.3: From left, 1: Probability density distribution of shear rate from the soundings of figure 4.2. 2: Averaged auto correlation functions indicating the vertical persistence of a given shear tendency (see text). 3: Histogram of tropopause temperatures, and scatter plot of tropopause temperature versus tropopause height. 4: Lapse rate and pressure profiles.

The shear can reach values up to hundreds of m/(s km) in narrow regions, while the mean value is only 7.2 m/(s km). Since the statistics of meridional and longitudinal wind-shear are almost identical we assume that the contrail spreading does not have a “preferred direction” in this area. Since the directions are arbitrary the wind statistics of figure 4.3 represents wind statistics projected orthogonally to an arbitrary oriented contrail. In figure 4.3, temperature characteristics are also shown.

Baseline simulation and variations

From the observations a baseline simulation is formed. The characteristics of initialization of this simulation is shown in table 4.1. In addition to the baseline simulation a set of single parameter variations is chosen, in order to examine the contrail characteristics dependency of different parameters. All cases are supersaturated and fulfills the requirements for contrail formation and persistence, so the outcome is a conditional characterization; if the conditions for contrails are there, how will they develop in time, and what are their optical properties. The MPC model is not able to simulate the initial turbulent phase, i.e the part where the vortices dies out, and where nucleation occurs. The dynamics of this phase has been simulated e.g. in [Gierens and Jensen, 1998]. Based on these simulations, and on comparison with measurements [Schröder et al., 2000], the initial width, height and particle size-distribution are chosen, in order to approximate a 15 minutes old contrail.

Results

In the simulations presented here the MPC model is executed in 2-d mode, with periodic boundary conditions horizontally. Due to the physical nature of contrail spreading it is not necessary to run in 3-d. The simulations includes a “baseline-simulation”, representing a typical contrails event. The accuracy of the baseline simulation has been tested with additional simulations with higher resolution, see 4.1. Low vertical resolution results in an apparent horizontal “wave” in the optical depth, which is identified as a result of different advection velocities of different layers. This effect does not lead to any error in the integrated clod parameters. Several additional simulations have been performed, all representing variations in the model input or simulation parameters, chosen to test the sensitivity of contrail formation.

	Baseline	Variations
Saturation Ratio	1.25	1.1
Wind shear	7.2m/(s km)	12.0 (90 deg)
Shear depth	0.25 km	0.45 km
Supersaturation depth	0.8 km	
Temperature	215 K at 9.5 km	224 K at 9.5 km and 216 K at 11.5 km
Tropopause/contrail height	9.5 km	10.5 km
Lapse	7.0 m/s km	9.8 m/s km
Initial particle density	$20/cm^3$	$100/cm^3$
Initial contrail width/height	400m/100m	800m/200m
Initial mean particle radius	2 μ m	10 μ m)
Initial log-normal stdv	1.25	
Ice water sticking coeff.	1.0	0.05
Ice particle aspect ratio	1.11	
Grid Resolution	66m $\times$ 19m	40m $\times$ 19m and 66m $\times$6.3m

Table 4.1: Properties of the baseline simulation. Last column are the variations chosen for sensitivity tests. “Shear depth” and “supersaturation depth” indicates the depth of the layer below the contrail, where these properties persists, before they are truncated. In table 4.2 the simulation denoted “216 K at 11.5 km” is refered to as “Tropical”.

Features of the baseline simulation

Generally the total number of particles is decreasing moderately during the first 2 hours, while the contrail is spreading. The size distributions varies a lot in space, with the larger particles (order of 40 μ m) at the bottom of the cloud and the smaller particles at top (see figure 4.4 (1)).

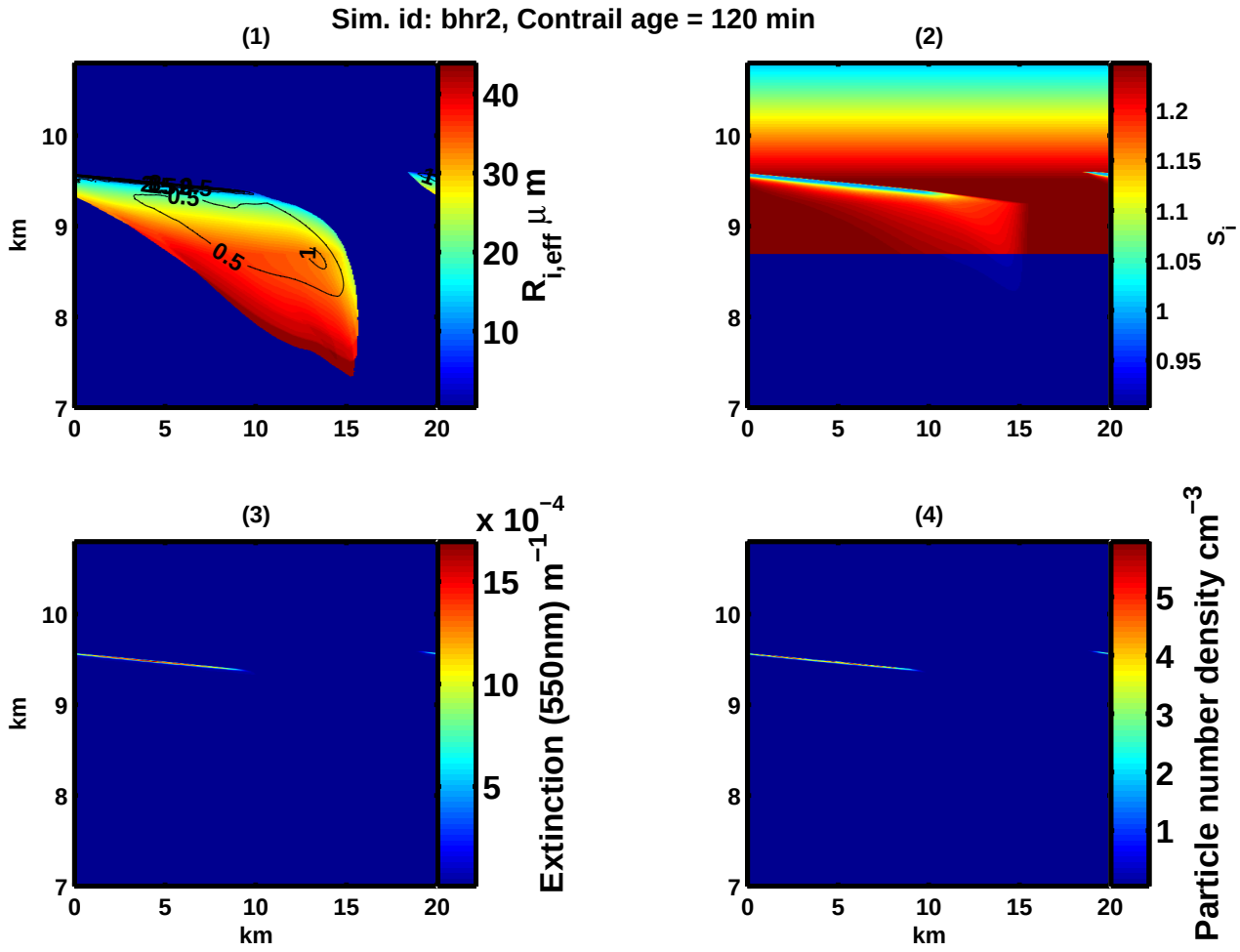

Figure 4.4: Features of the baseline simulation. Black contours in first plot denotes ice water content (mg/m^3)

The number density remains fairly high, i.e. up to 8 particles per cm^3 at the cloud top even after 2 hours of existence. The total ice water content (IWC) also has its maximum at the cloud top. However, the IWC is growing to 1 mg/m^3 in the fall streak, even though the number density is very low there. This leads to a relative small but significant contribution to the extinction coefficient and optical depth of the cloud 8-10 kilometers from the contrail core. In figure 4.5 the vertical optical depth across the contrail is plotted at different times. The optical depth is very low, starting at around 0.11 at time = 0 h, decreasing to 0.02-0.03 after two hours.

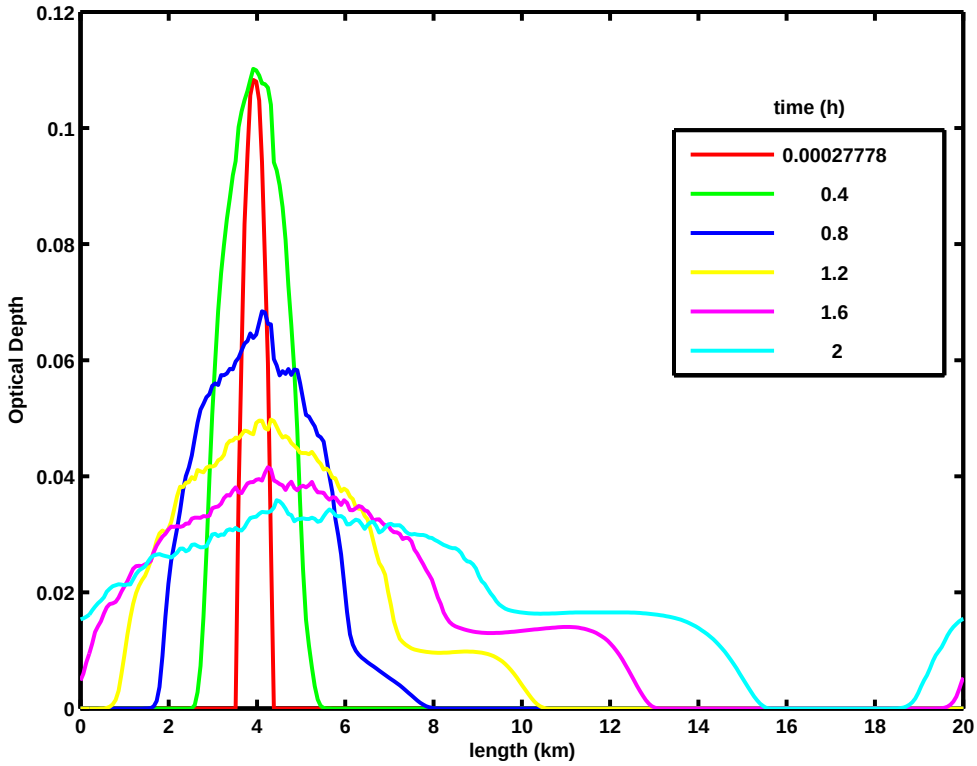

Figure 4.5: Vertical baseline optical depth of scattering at 550 nm.

Features of variation ensemble.

In addition to the baseline simulation, 11 other simulations are presented. Short descriptions of the simulations are found in table 4.2. In order to overview the differences between various perturbations a few feature variables are defined: The total ice water cross section i.e. the IWC per unit length along the contrail is calculated by integrating IWC over the contrail cross section. See figure 4.7. Three simulations are strikingly different from the main group: $S_i = 1.1$ gives significantly smaller IWC. The $T = T + 9$ K simulation and the "Tropical" simulation which is performed with $T = 230$ K at flight altitude, gives much higer IWC.

Likewise a variable, "the total extinction" ,W, is defined by integrating the optical depth horizontally. It's dimension is length. And even though W doesn't represent the actual geometrical width of the contrail, it can give an idea about the overall impact of the contrail. W is plotted as function of time in figure 4.8. Again the tropical simulation gives high numbers. The red dashed curve is a contrail which is initiated which much bigger ice crystals (10 μ) and consequently it has higher extinction coefficient from the beginning. Finally the mean effective radius $R_{i,eff}$ weighted with IWC is calculated as function of time and plotted in figure 4.9. Here the same pattern is seen. The tropical simulation stabilizes at $R_{i,eff} = 45 - 47\mu$m in one hour, in contrast to the baseline which reaches a value around 17 μm in one hour.

	τ_0	IWC_0	$R_{i,eff,0}$	Simulation−id
——	1.00	1.14	1.10	lapse 9.8 K/km
——	0.50	6.00	1.80	Tropical
——	0.62	3.00	1.50	T = T+9K (Midlat.)
——	1.05	1.00	1.00	450m shear field
——	1.00	1.05	1.10	Height 10.5 km
——	1.00	1.00	1.00	baseline
——	1.00	1.07	1.00	Initial Ice P. density 100 cm^{-3}
- - - -	0.67	1.10	1.00	Initial Mean Radius 10.0 μ m *
- - - -	1.35	4.00	1.10	Initial width of contr. 800 m× 200 m
- - - -	1.20	1.10	1.00	Sticking coefficient 0.05
- - - -	1.40	0.38	0.73	Saturation ratio (ICE) 1.1
- - - -	0.95	1.22	1.00	Wind shear 12.0 (m/(s km))

Table 4.2: Color codes for figure 4.7 to 4.10. The number columns are: 1) Time scale factor and 2) IWC scale factor. See figure 4.6 for visualization of the individual simulations.

In order to characterize the differences between the baseline and the individual simulations, the time scale and IWC, and $R_{i,eff}$ are scaled for each simulation to match the baseline. The scaling factors are printed in table 4.2. It is not a physically justified scaling law, merely a practical way to illustrate a possible way of parameterizing contrails. All scaled IWC functions are plotted on top of each other in figure 4.10. In figure 4.9 the same time-scaling is used in an attempt to scale $R_{i,eff}$ with success in all cases except for one case, namely the simulation with initial mean radius set to 10 μm. This means that a parameterization derived from these simulations is sensitive to the assumed initial particle size. However, 10 μ m is an unrealistic high particle size for a 15 minutes contrail age. The baseline simulation only reach this mean value at the age of one hour. This is because the particle growth is limited by the spatial extend of the contrail, which is mainly increasing as a result of sedimentation; the larger volume covered, the more water available for ice deposition.

To summarize: The MPC simulations suggest that long lived contrails may be parameterized by a crude estimate of $R_{i,eff}$ and IWC as functions of time, depending mainly on local temperature, humidity and initial cross section and mean particle radius. The simulations also implies that the optical parameters of contrails depends significantly on latitude, with much higher IWC and $R_{i,eff}$ close to equator that near the poles.

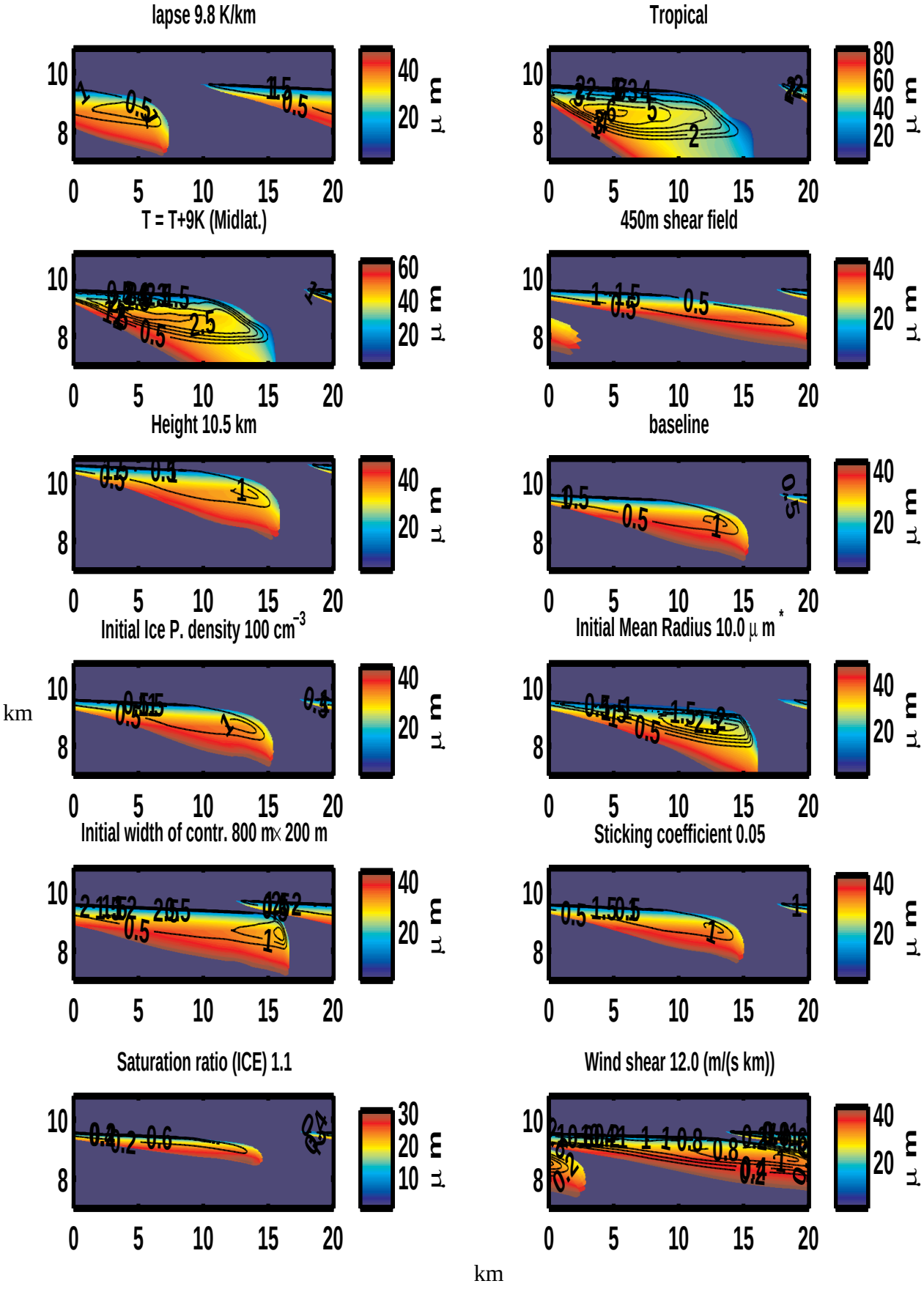

Figure 4.6: IWC (black contours units: mg/m^3) and $R_{i,eff}$ (color-scale) of 12 different simulations. The coordinate units are km.

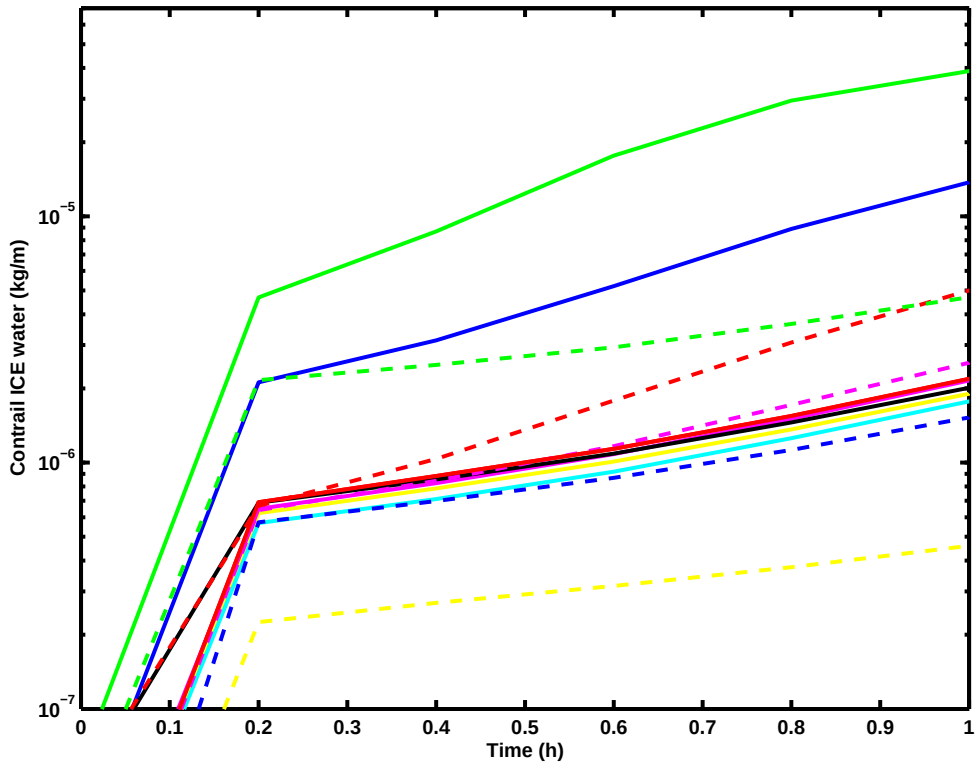

Figure 4.7: Total contrail ice water content [kg/m] as function of time

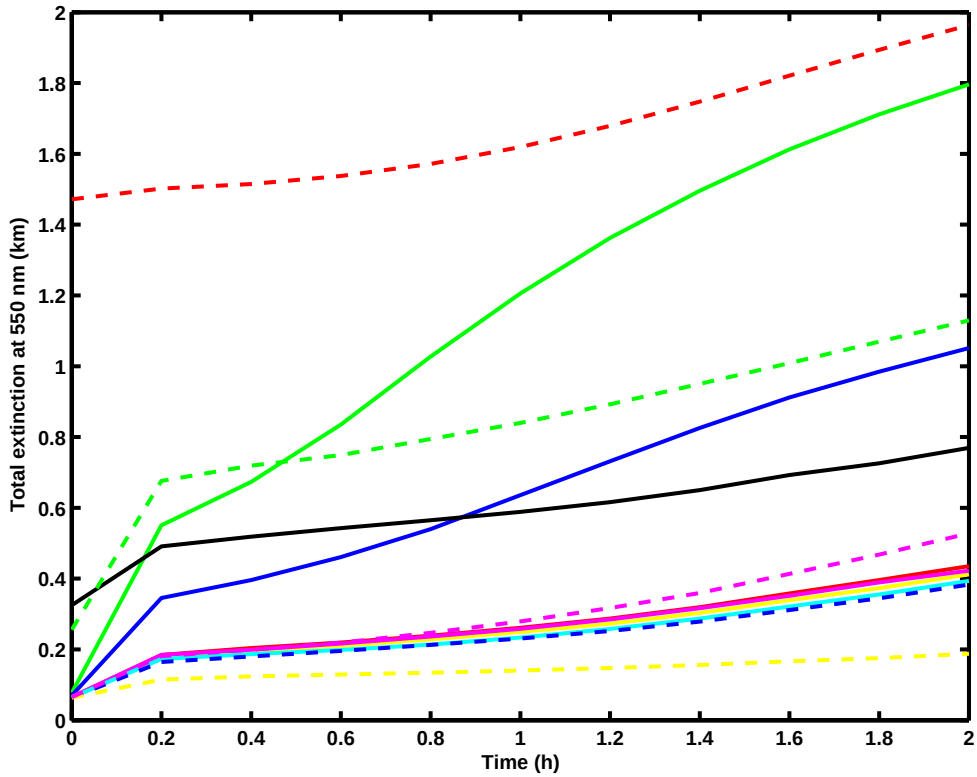

Figure 4.8: Total extinction at 550 nm . The descriptions are found in table 4.2

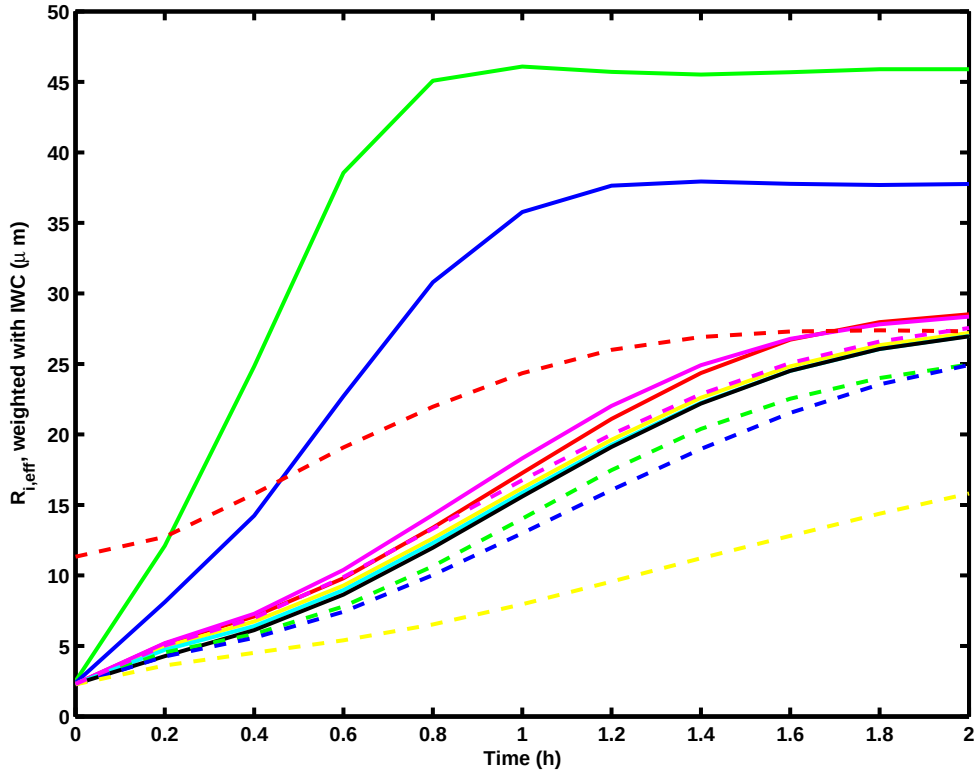

Figure 4.9: Effective radius weighted by IWC [μ m]

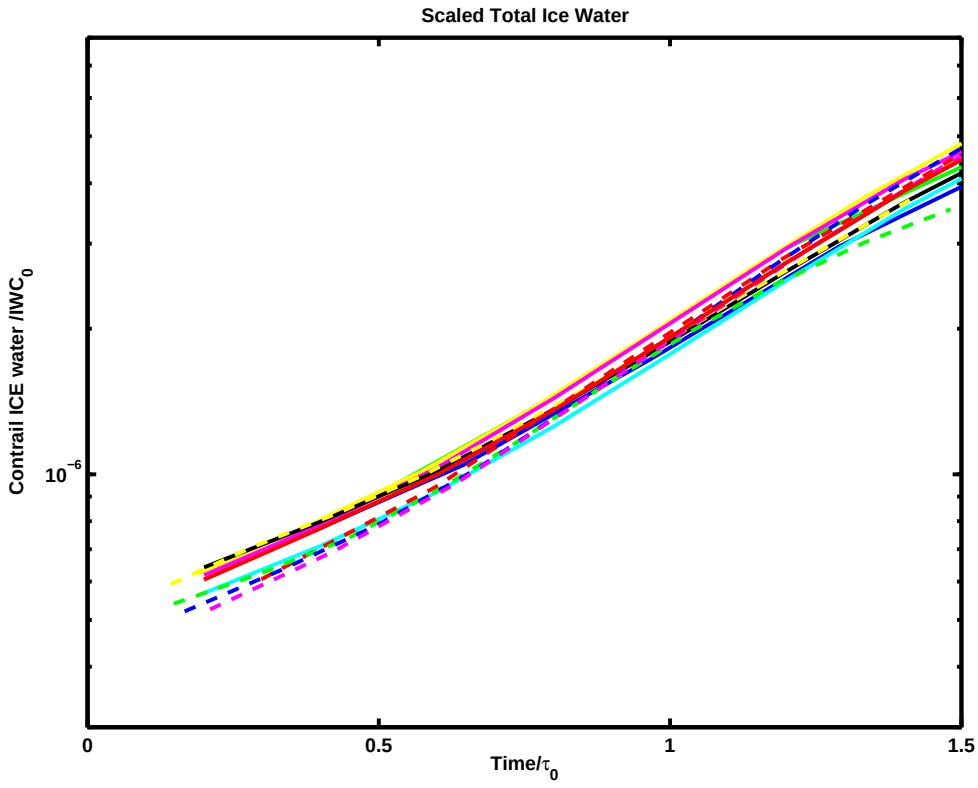

Figure 4.10: Scaled total contrail ice water content as function of scaled time.

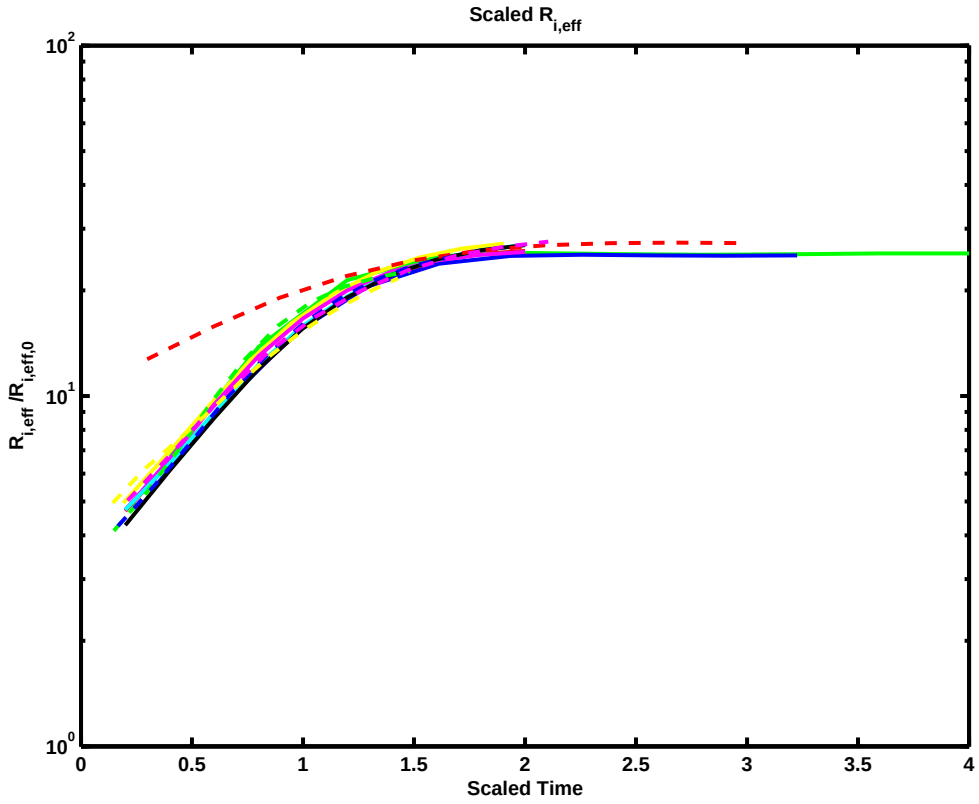

Figure 4.11: Scaled effective radius as function of scaled time.The simulation with initial mean radius = 10 μm does not obey the scaling law. I.e., it is not possible to reduce the time scale for $R_{i,eff}$ and IWC with the same constant, τ, see text.

Conclusions

The physical properties of contrails has been studied through microphysical simulations featuring the interplay between size distributions, sedimentation, shear, deposition, sublimation etc.

Simulations of contrail events in 12 different situations, surrounding a baseline simulation, resembling a typical winter profile of the north Atlantic at approximately 60deg latitude were run for 2 hours.

The optical depth at 0.55 μ m decreases from 0.11 to 0.05 in the first hour of simulation. Generally the optical depth is largest in the contrail core. The fall streaks has an optical depth below 0.02, but around 2 hours into the simulation it increases to above 0.02, and approaches the optical depth of the contrail core, around 0.03.

The sensitivity studies was used to extract empirical scaling relations, for the time dependent effective radius and ice water content, suggesting a route for parameterization of contrails developing into cirrus clouds.

The largest sensitivity is observed on changes in humidity, temperature and wind shear. Humidity and temperature essentially acts through the same mechanism; since contrails is formed when the relative humidity is around 100 % and above, and since absolute humidity increases fast with temperature, larger temperatures usually corresponds to larger amounts of water vapor available for depositional growth.

The effective radius is doubled, from around 16 μm at after 1 hour, to around 32 μm if the contrail core temperature is increased 9 K from 215 K to 224 K, and up to 45-47 μm if the temperature is raised to 230 K. The same variable is decreased from 16 μm to 7 μm if the initial relative humidity is set to 110% instead of 125%.

Change of wind shear does not influence much on effective radius or ice water content during the 2 hour simulation, but the horizontal width of the contrail increases with the wind shear. A wind shear rate of 7.2 m/(s km), which is the average magnitude around the tropopause in the north Atlantic results in a smearing to approximately 5 km after 1 hour.

Discussion and Conclusions

Comparison between MPC and IFSHAM

The contrail parameterization employed in IFSHAM is based on satellite observations of linear, i.e. young contrails. Disregarding the fact that older contrails has greater impact according to the MPC model, we shall restrict the comparison to younger contrails. The IFSHAM winter mean optical depth in the north Atlantic is between 0.02 and 0.05, which is less than the prediction of the MPC baseline simulation; assuming that the contrails are less than one hour old, the MPC baseline simulation predicts optical depth to be 0.05 to 0.11 during the first hour. However, in the nudged IFSHAM simulations (where the model systematic errors are minimized) the winter mean of the optical depth in the north Atlantic is between 0.02 and 0.1 and therefore corresponds better to the MPC baseline simulation. In the MPC simulations, the optical depth is very sensitive to initial humidity, and the simulation with $S_i = 1.1$ predicts smaller optical depth values than the baseline simulation. (Initialization of the humidity in the MPC simulations was based on radio-soundings, which are not reliable near the tropopause.)

The winter mean of the effective radius of particles in the north Atlantic UTLS, as predicted by IFSHAM lies in the area of 14-17 μm, whereas the ECHAM4 model predicts average radii in the interval 12-13 μm. The mean of MPC effective radius from the same period is lower. This may have to do with the initialization of MPC; the test run initialized with larger particles ($r = 10\mu$m) actually lies above the IFSHAM values. After 1.3 hour the effective radius difference between the two MPC initializations vanishes.

The MPC simulations with larger temperatures illustrates what happens in the tropics: The higher temperatures leads to more excess water, and bigger effective radii. This is also captured by IFSHAM, but this feature is absent in the average values predicted by the ECHAM4 parameterization. Specifically in the 230 K simulation, which corresponds to a tropical profile the effective radius increases from 2 to almost 50 μm, which is consistent with average values of 20-25 μm as determined by IFSHAM in the tropical regions.

So in terms of variability and latitude dependency IFSHAM and MPC are consistent, while the ECHAM4 parameterization has a much smaller latitude dependency.

References

[Appleman, 1953] Appleman, H. (1953). The formation of exhaust condensation trails by jet aircraft. *Bull. Am. Meteorol. Soc.*, 34:14–20.

[Bakan et al., 1994] Bakan, S., Gothe, M. B., Gayler, V., and Grassl, H. (1994). Contrail frequency over Europe from NOAA-satellite images. *Ann. Geophys.*, 12:962–968.

[Del Guasta and Niranjan, 2001] Del Guasta, M. and Niranjan, K. (2001). Observation of low-depolarization contrails at Florence (Italy) using a 532-1064 nm polarization LIDAR. *Geophysical Research Letters*, 28:4067–4070.

[Déqué et al., 1994] Déqué, M., Dreveton, C., Braun, A., and Cariolle, D. (1994). The arpege/ifs atmosphere model: a contribution to the french community climate modelling. *Climate Dynamics*, 10:249–266.

[Eliasen et al., 1970] Eliasen, E., Machenhauer, B., and Rasmussen, E. (1970). *On a numerical method for integration of the hydrodynamical equations with a spectral representation of the horizontal fields*. Report no. 2. Institute for Theoretical Meteorology, Copenhagen University, Copenhagen, Denmark.

[Fortuin et al., 1995] Fortuin, J. P. F., van Dorland, R., Wauben, W. M. F., and Kelder, H. (1995). Greenhouse effect of of aircraft emissions as calculated by a radiative transfer model. *Ann. Geophys.*, 13:413–418.

[Fouquart and Bonnel, 1980] Fouquart, Y. and Bonnel, B. (1980). Computations of solar heating of the earth's atmosphere: A new parameterization. *Beitr. Phys. Atmos.*, 53:35–62.

[Gibson et al., 1997] Gibson, J. K., Kå llberg, P., Uppala, S., Hernandez, A., Nomura, A., and Serrano, E. (1997). *ERA-15 Description*, volume 1 of *ECMWF Re-analysis Project Report Series*. ECMWF, Reading, U.K.

[Gierens and Jensen, 1998] Gierens, K. and Jensen, E. (1998). A numerical study of the contrail-to-cirrus transition. *Geophysical Research Letters*, 25(23):4341–4.

[Guldberg et al., 2004] Guldberg, A., Kaas, E., Deque, M., Yang, S., and Thorsen, S. V. (2004). Reduced systematic errors by empirical model correction; impact on seasonal prediction skill . *Tellus A*. Accepted.

[Heymsfield et al., 1998] Heymsfield, A. J., Lawson, R. P., and Sachse, G. W. (1998). Growth of ice crystals in a precipitating contrail. *Geophysical Research Letters*, 25:1335–1338.

[IPCC, 1999] IPCC (1999). *Aviation and the global atmosphere*. Cambridge University Press, Cambridge, UK.

[Jensen et al., 1998] Jensen, E. J., Ackerman, A. S., Stevens, D. E., Toon, O. B., and Minnis, P. (1998). Spreading and growth of contrails in a sheared environment. *jgr*, 103(.12):31557–31568.

[Jeuken et al., 1996] Jeuken, A. B. M., Siegmund, P. C., Heijboer, L. C., Feichter, J., and Bengtsson, L. (1996). On the potential of assimilating meteorological analyses in a global climate model for the purpose of model validation. *J. Geophys. Res.*, 101:16939–16950.

[Larchevêque et al., 2002] Larchevêque, G., Balin, I., Quaglia, P., Nessler, R., Simeonov, V., van den Bergh, H., and Calpini, B. (2002). Optical Properties of Aerosols - Clouds - Contrails and Water Vapor Mixing Ratio By Lidar From The Jungfraujoch Research Station (3580 M Asl). *EGS XXVII General Assembly, Nice, 21-26 April 2002, abstract #5820*, 27:5820–+.

[Larsen, 2000] Larsen, N. (2000). Polar stratospheric clouds - microphysical and optical models. *Tecnical Report, DMI*, 00-06.

[Lawson et al., 1998] Lawson, R., Heymsfield, A., Aulenbach, S., and Jensen, T. (1998). Shapes, sizes and light scattering properties of ice crystals in cirrus and a persistent contrail during SUCCESS. *Geophysical Research Letters*, 25(9):1331–4.

[Lohmann and Roeckner, 1996] Lohmann, U. and Roeckner, E. (1996). Design and performance of a new cloud microphysics scheme developed for the echam general circulation model. *Climate Dynamics*, 12:557–572.

[Mannstein and Schumann, 2004] Mannstein, H. and Schumann, U. (2004). Observations of Contrails and Cirrus over Europe. In Robert Sausen, C. F. and Amanatidis, G., editors, *"Aviation, Atmosphere and Climate"*, number 83 in Air pollution research report, pages 244–248. European Commission.

[Marquart, 2003] Marquart, S. (2003). *Klimawirkung von Kondensstreifen: Untersuchungen mit einem globalen atmosphaerischen Zirkulationsmodell*. Dissertation der Fakultaet fur Physik der Ludwig-Maximilians-Universitae Munchen. Deutsches Zentrum fur Luft- und Raumfahrt., Oberpfaffenhofen, Germany.

[Marquart and Mayer, 2002] Marquart, S. and Mayer, B. (2002). Towards a reliable GCM estimation of contrail radiative forcing. *Geophysical Research Letters*, 29:20–1–20–4.

[Marquart et al., 2003] Marquart, S., Ponater, M., Mager, F., and Sausen, R. (2003). Future Development of Contrail Cover, Optical Depth, and Radiative Forcing: Impacts of Increasing Air Traffic and Climate Change. *Journal of Climate*, 16:2890–2904.

[Meerkotter et al., 1999] Meerkotter, R., Schumann, U., Doelling, D. R., Minnis, P., Nakajima, T., and Tsushima, Y. (1999). Radiative forcing by contrails. *Ann. Geophys.*, 17:1080–1094.

[Meyer et al., 2001] Meyer, R., Mannstein, H., and Wendling, P. (2001). Regional Frequency of Contrails Derived from Satellite Data and their Radiative Forcing. In Schumann, U. and Amanatidis, G., editors, *"Aviation, aerosols, contrails and cirrus clouds"*, number 74 in Air pollution research report, pages 230–234. European Commission.

[Minnis et al., 2004] Minnis, P., Kirk Ayers, J., Palikonda, R., and Phan, D. (2004). Contrails, cirrus trends, and climate. *Journal of Climate*, 17:1671–1685.

[Minnis et al., 1998] Minnis, P., Young, D. F., Garber, D. P., Nguyen, L., Smith, W. L., and Palikonda, R. (1998). Transformation of contrails into cirrus during SUCCESS. *Geophysical Research Letters*, 25:1157–1160.

[Minnis et al., 1999] Minnis, P. Schumann, U., Doelling, D. R., Gierens, K. M., and Fahey, D. (1999). Global distribution of contrail radiative forcing. *Geophysical Research Letters*, 26:1853–1856.

[Mlawer et al., 1997] Mlawer, E. J., Taubman, S. J., Brown, P. D., Ianoco, M. J., and Clough, S. A. (1997). Radiative transfer for inhomogenous atmospheres: Rrtm, a validated correlated-k model for the longwave. *Journal of geophysical research*, 102:16663–16682.

[Morcrette, 1991] Morcrette, J.-J. (1991). Radiation and cloud radiative properties in the europen centre for medium range weather forecasts forecasting system. *J. Geophys. Res.*, 96:9121–9132.

[Nielsen, 2004] Nielsen, J. K. (2004). 3-D simulation of contrail to cirrus transition, - the onset of sedimentation. In *"Aviation, Atmosphere and Climate"*, number 83 in Air pollution research report, pages 279–281. European Commission.

[Ponater et al., 2002] Ponater, M., Marquart, S., and Sausen, R. (2002). Contrails in a comprehensive global climate model: Parameterization and radiative forcing results. *Journal of Geophysical Research (Atmospheres)*, 107(D13):ACL 2 1–15.

[Raisanen, 1998] Raisanen, P. (1998). Effective longwave cloud fraction and maximum-random overlap of clouds: A problem and a solution. *Mon. Weather Rev.*, 126:3336–3340.

[Roeckner et al., 1996] Roeckner, E., Arpe, K., Bengtsson, L., Christoph, M., Clausse, M., Dumenil, L., Esch, M., Giorgetta, M., Schlese, U., and Schulzweida, U. (1996). The atmospheric general circulation model echam-4: Model description and simulation og present-day climate. *Max-Planck-Inst. Meteorol. Rep.*, 218:99 pp.

[Roeckner et al., 2003] Roeckner, E., Bäuml, G., Bonaventura, L., Brokopf, R., Esch, M., Giorgetta, M., Hagemann, S., Kirchner, I., Kornblueh, L., Manzini, E., Rhodin, A., Schlese, U., Schulzweida, U., and Tompkins, A. (2003). The atmospheric general circulation model echam 5. part i: Model description. *Max-Planck-Inst. Meteorol. Rep.*, 349.

[Sausen et al., 2004] Sausen, R., Fichter, C., and Amanatidis, G., editors (2004). *Aviation, Atmosphere and Climate*, number 83 in Air pollution research report. European Commission.

[Schmidt, 1941] Schmidt, E. (1941). Die Entstehung von Eisnebel aus den Auspuffgasen von Flugmotoren. In Oldenbourg, R., editor, *"Schriften der Deutschen Akademie der Luftfahrt-forschung"*, volume 44, pages 1–15, Munich, Germany.

[Schmitt and Brunner, 1997] Schmitt, A. and Brunner, B. (1997). Emissions from aviations and their development over time. In Schumann, U., editor, *"Pollutants From Air Traffic - Results of Atmospheric Research 1992-1997"*, number 97-04 in DLR-Forschungsber., pages 27–52, Cologne, Germany. Deutsches Zentrum für Luft- und Raumfahrt.

[Schröder et al., 2000] Schröder, F., Kärcher, B., Duroure, C., Ström, J., Petzold, A., Gayet, J.-F., Strauss, B., Wendling, P., and Borrmann, S. (2000). On the Transition of Contrails into Cirrus Clouds. *Journal of Atmospheric Sciences*, 57:464–480.

[Schumann, 1996] Schumann, U. (1996). On conditions for contrail formation from aircraft exhausts. *Meteorol. Z.*, 5:4–24.

[Schumann, 2000] Schumann, U. (2000). Influence of propulsion efficiency on contrail formation. *Aerosp. Sci. Technol.*, 4:391–401.

[Sundqvist, 1978] Sundqvist, H. (1978). A parameteraization scheme for non-convective condensation including predcition of cloud water content. *Q. J. R. Meterol. Soc.*, 104:677–690.

[Sundqvist et al., 1989] Sundqvist, H., Berge, E., and Kristjansson, J. E. (1989). Condensation and cloud parameterization studies with a mesoscale numerical weather prediction model. *Mon. Weather Rev.*, 117:1641–1657.

[Tompkins, 2002] Tompkins, A. M. (2002). A prognostic parameterization for the subgrid-scale variability of water vapour and clouds in large-scale models and its use to diagnose cloud cover. *Journal of the atmospheric sciences*, 59:1917–1942.

[UWYO, 2004] UWYO (2004). http://weather.uwyo.edu/upperair/sounding.html.

[Walcek, 2000] Walcek, C. J. (2000). Minor flux adjustment near mixing ratio extremes for simplified yet highly accurate monotonic calculation of tracer advection. *Journal of Geophysical Research*, 105:9335–9348.

[Wang et al., 2003] Wang, J., Carlson, D. J., Parsons, D. B., Hock, T. F., Lauritsen, D., Cole, H. L., Beierle, K., and Chamberlain, E. (2003). Performance of operational radiosonde humidity sensors in direct comparison with a chilled mirror dew-point hygrometer and its climate implication. *Geophysical Research Letters*, 30:11–1.

[Yang, 2004] Yang, S. (2004). The DKCM Atmospheric Model. The Atmospheric Component of the Danish Climate Model. Danish Climate Centre Report 04-05, DMI, Denmark.

Previous reports

Previous reports from the Danish Meteorological Institute can be found on:
http://www.dmi.dk/dmi/dmi-publikationer.htm